Spring 1-1-2011

Characterization of Viscoelastic Behaviors in Bovine Pulmonary Arterial Tissue

Gregory James Pelkie
University of Colorado at Boulder, gregory.pelkie@colorado.edu

Characterization of Viscoelastic Behaviors in Bovine Pulmonary Arterial Tissue

written by

GREGORY JAMES PELKIE

B.S., Michigan State University, 2009

A thesis submitted to the

Faculty of the Graduate School of the

University of Colorado in partial fulfillment

of the requirement for the degree of

Master of Science

Department of Mechanical Engineering

2011

This thesis entitled:

Characterization of Viscoelastic Behaviors in Bovine Pulmonary Arterial Tissue

written by Gregory James Pelkie
has been approved for the Department of Mechanical Engineering

_____
Professor J. Hang Qi

_____
Professor Wei Tan

*Date*_____

The final copy of this thesis has been examined by the signatories, and we Find that both the content and the form meet acceptable presentation standards Of scholarly work in the above mentioned discipline.

ABSTRACT

Pelkie, Gregory James (M.S., Mechanical Engineering)

Characterization of Viscoelastic Behaviors in Bovine Pulmonary Arterial Tissue

Thesis directed by Associate Professor J. Hang Qi

This work presents a characterization of the influence of viscoelasticity on the mechanical behavior of bovine pulmonary arteries. It is commonly accepted that biological soft tissues do indeed exhibit viscoelastic characteristics; however its effect has yet to be quantified. Stress relaxation tests are used to determine the time dependent response of bovine pulmonary tissue. Fitting this data to a modified standard linear solid model, allows a total of five independent time constants are attained, each of which describe individual time scales on which the medium has a viscoelastic response to an applied strain. These time constants are applied to an analytical model through the Boltzmann integral in order to describe the stress response to a prescribed loading strain. The strain used in this case was a sine wave in order to mimic the *in vivo* flow of blood from the heart. These results were also modeled using finite element simulations in order to verify the time dependent response. It was found that although viscoelasticity is a necessary consideration, depending on the loading conditions, it may in some cases be either neglected or simplified. A time scale at which testing should be done in order to reduce time dependent effects as well as a simplified model describing the viscoelastic effect on the ultimate tissue response is presented.

ACKNOWLEDGEMENTS

I would like to express my appreciation to my thesis advisor Dr. J. Hang Qi for giving me the opportunity to join his team and for his guidance and expertise. Most importantly, he provided me with support and encouragement throughout this process. I also would like to send my thanks to my thesis committee members: Dr. Mark Rentschler and Dr. Wei Tan. I am thankful that amidst their busy schedules, they accepted to be members of my thesis committee.

This work also would not have been possible without the help of Phil Kao, Steve Lammers, and Lian Tian. Their previous work and collaboration allowed me to gain a much stronger knowledge base on the topic of arterial mechanics. I would especially like to thank Phil for his valuable scientific advice and constructive comments. I also appreciate the many hours spent by Stacey Sokol in the lab. Without her help, these time consuming experiments would not have been possible. I also am very grateful to Arapahoe Meat Packing for generously allowing me to collect pulmonary tissues.

Finally, I would like to thank my friends and family. Kelly Hall has been very supportive throughout the ups and downs, and has displayed great confidence in me. Last but not least, my parents deserve special mention for they have bestowed in me the importance of learning and succeeding. Thank you.

CONTENTS

List of Tables vi
List of Figures vii
I. Introduction 1
II. Background 3
Biology Background 3
Material Properties 5
Preconditioning 6
Viscoelasticity 12
Pressure-Diameter Relationship 16
III. Experiments 18
Experimental Background 18
Materials and Methods 18
Sample Preparation 18
Experimental Method 19
Data Fitting 20
Results 21
Typical Stress Response 21
Grouped Stress Response 23
Effects of Strain Levels 25
Effects of Locations 26
Effects of Directions 27
Experimental Results 29
IV. Modeling 32
Novel Model from Stress Relaxation Experiment 32
Finite Element Verification 39
V. Conclusion 49
Bibliography 51
Appendix 55
Analytical Matlab Model 55
Abaqus Input File 58

LIST OF TABLES

Table 1. *Average and standard deviation of all time constants as determined by Prony series curve fitting.* 24

Table 2. *Matlab model input parameters.* 36

Table 3. *Fitting parameters for Ogden material model* 41

Table 4. *Experimentally obtained Prony series parameters used for the Abaqus material model* 42

LIST OF FIGURES

Figure 1. *Diagrammatic scheme of the layered structure within the wall of an elastic artery adapted from [9].* 4

Figure 2. *Figure 2A shows the variation between the stress and strain responses of the same tissue over cycles 1 through 10. Figure 2B shows only cycle 1 and 10 of the preconditioning cycle. It can be observed that the loading and unloading path become increasingly similar until the curves become nearly repeatable.* 7

Figure 3. *Stress–strain responses of spinal cords subjected to uniaxial strain of 2% (groups 2 and 3) and 5% (group1). While specimens of groups 1 and 2 were preconditioned to 5% strain, specimens of group 3 were preconditioned to a lower strain of 2% [14]*.....10

Figure 4. *Load preconditioning curves from the same specimen shown in Fig. 6, after conclusion of the stress relaxation tests. Note that the 25 load preconditioning cycles plotted for each day are virtually identical, indicating that the specimen remains in a load-preconditioned state after each sequence of stress relaxation. There is evidence, however, of specimen lengthening (~6%) over the course of 3 days of testing [11]*.....11

Figure 5. *Schematic protocol with three stress levels: low (0.025 MPa), med (0.05 MPa) and high (0.1 MPa). Relaxation time = 1 hour. Loading rate during preconditioning ramps: 0.03 mm s^{-1} [23]*.....14

Figure 6. *Ramp and stress relaxation example for specimen PH45 during stress level HIGH. Measured data in solid line and model fitting in dots. The difference (Error) between them is also drawn as a solid line. A magnified area of the peak and initial relaxation portions is shown the center of the figure.* 15

Figure 7. *Comparison of vessel behavior (axial weights are 5 gram and 25 gram, respectively). Both the control and balloon-induced vessels stiffened with increased axial loads [28]*.....17

Figure 8. *Normalized stress relaxation response for the circumferential and longitudinal directions. The observed stress for the 65% strain case falls to below 70% of the initial stress as time approaches 1200 seconds. It is seen that even with low constant strain, the final stress response is less than 80% of original. The rate at which the stress decreases becomes linear at approximately 300 seconds in all of the cases.* 22

Figure 9. *Sample curve fit of the Prony series model to the experimental relaxation data. Initially, the data was fit to a two Prony series model however it was found that five Prony series were necessary to capture the strong initial relaxation of the tissue.* 22

Figure 10. *Histograms of the pooled time constants for all of the gathered data. The data follows a relatively normal distribution curve. No major trends were observed between the tissue locations (MPA, RPA, LPA) nor the direction (circumferential, longitudinal).*.....23

Figure 11. *Plot of the grouped branch moduli with standard deviations. The moduli were found by fitting the 5 term Prony series (Eq. 2). The moduli corresponding to the fastest time constants are generally lower in magnitude than are the moduli related to the slower time constants.*.....24

Figure 12. *Semi-log scale plot of the grouped relaxation times with standard deviations. The standard deviations are relatively small suggesting that the time scale my not significantly differ between either tissue location or tissue direction.* 25

Figure 13. *Plots of the average moduli in relation to the test strain. The data set chosen for these plots was that from the MPA in the circumferential direction. It can be seen from the plots that there is no strong correlation between the observed moduli and the strain at which the test was performed.* 26

Figure 14. *Plots of the average time constants as a function of test strain. The data set chosen for these plots was that from the MPA in the circumferential direction. It can be seen from the plots that there is no correlation between the observed relaxation times and the strain at which the test was performed.* 26

Figure 15. *Plots of the average moduli in relation to the tissue direction. The data set chosen for these plots was that from the circumferential direction taken at 55% strain. It seems as though the RPA produces the highest moduli followed by the LPA and MPA respectively.* 27

Figure 16. *Plot of time constant data for the MPA, RPA, and LPA in the circumferential direction at 55% test strain. As expected, there is little variation in the relaxation time scale between the three tissue types.* 27

Figure 17. *Plots of the average moduli in relation to the test strain. The data set chosen for these plots was that from the MPA at 55% test strain. It can be seen from the plots that there is no strong correlation between the observed moduli and the direction of the tissue, although the circumferential direction does provide slightly stiffer average moduli in all cases.* 28

Figure 18. *Plots of the average time constants as a function of test strain. The data set chosen for these plots was that from the MPA at 55% test strain. It can be seen from the plots that there is no correlation between the observed relaxation times and the strain at which the test was performed.* 28

Figure 19. *Matlab simulation of the stress-strain response using the cyclic strain input (with a linear initial loading ramp) described in Equation (4.21). The simulation was run until t = 10^5 seconds. This result is compared against Equation (4.22), which is the simplification for the stress response to the same input as t approaches infinity.*.....36

Figure 20. *Matlab model predicted stress-strain response for each individual Maxwell element. The stress decreases to equilibrium as time becomes large. It can also be seen that the predicted response from Equation (4.22) fits very well for each of the individual branches.*.....37

Figure 21. *Matlab model ultimate predicted stress-strain response with added smooth muscle branch. The time constants for the smooth muscle effects was equal to τ_1 and the smooth muscle branch modulus was varied between 5, 10, 20, and 30% strain from top left to bottom right respectively. With a smaller modulus, the hysteresis loop is much smaller when compared to larger values of E_s.*.....39

Figure 22. *Abaqus model fit for the Ogden material model against experimentally obtained uniaxial stress strain behavior. The Ogden model fits soft tissue very well when using N=3.*.....42

Figure 23. *Applied pressure profile used for the finite element simulations. There is an initial loading ramp followed by a sine oscillation at about 95 Hz. The oscillation pressures vary from 10 kPa to 16 kPa or about 80 to 120 mmHg. These parameters are chosen to simulate biological loading conditions.*.....44

Figure 24. *The stress profile contour plot of the arterial section at peak deformation. The stress decreases from about 14.4 kPa on the inner surface of the vessel to 0.37 kPa seen by the outer surface of the wall.*.....45

Figure 25. *The displacement profile contour plot of the arterial section at peak deformation. The displacement decreases from about 6.3 mm on the inner surface of the vessel to 5.0 mm along the exterior of the wall. These displacements compare favorably with the findings in Chapter III.*.....46

Figure 26. *The pressure-diameter response for the Ogden model using the parameters listed in Table 3. The diameter was calculated using the initial radius and the displacement data. It can be seen that the artery does relax from 100 to 1000 seconds and again from 1000 seconds to 10,000 seconds. The artery P-D response is at steady state after 10,000 seconds and reaches a repeatable loop.*.....47

Figure 27. *The pressure-diameter response for the modified Ogden model using the parameters listed in Table 3 as well as a smooth muscle term. The smooth term was just an added Maxwell element with a time constant equal to τ_1 (0.39sec) and a modulus value equal to 20% of E_0 (13.36 kPa). The diameter was calculated using the initial radius and the displacement data. It can be seen that the artery does relax from 100 to 1000 seconds and again from 1000 seconds to 10,000 seconds. The artery P-D response is at steady state after 10,000 seconds and reaches a repeatable loop. In the case of the added smooth muscle term it is obvious from the plot on the right that some sort of P-D loop does indeed exist. These results agree favorably with those seen from the Matlab simulations in Chapter III.* 48

CHAPTER I

I. Introduction

One of the major causes of death in the modern world is cardiovascular disease [1]. For this reason, much effort is put forth in order to model and explain the mechanics which govern both physiological and pathophysiological arterial states. Currently, it is not possible to completely model cardiovascular system function or a response which accurately reflects each of the physiologic phenomena taking place in vessels. However, the ever increasing computational capabilities of computers and the advancement of mechanics are allowing models to become more and more accurate. These arterial models are typically aimed at a better understanding of arterial diseases, including hypertension, aneurisms, and atherosclerosis as well as for design of treatment devices such as the angioplasty, stent, bypass, or graft [1].

These aforementioned reasons make it important to have a suitable constitutive model to utilize when creating a structural model accurately describing pulmonary arterial function. Viscoelasticity is the main mechanical component of arterial function which has yet to be widely considered in soft tissue constitutive models [1-4]. For accuracy, there are ever increasing numbers of fitting parameters in recent models [5], in which case, adding variables to account for viscoelasticity would increase this complexity to an even further extent. For this reason, it is of vast importance to determine the extent of viscoelasticity's role during *in vivo* mechanical loading. Also, development of a simplified approximation which would account for the viscoelastic behavior could be of great significance.

This work presents an analysis on the influence of viscoelastic behavior on bovine pulmonary arterial mechanics. Using a modified standard linear solid model, the stress relaxation response curves of the tissue can be fit allowing characterization of the viscoelastic response. Stress relaxation tests have been proposed to examine the time dependent behavior or

arterial tissue [6-11]. Fitting this data to the modified standard linear solid model allows both the moduli and time constants to be quantified [4, 8, 12]. Once the time dependent behavior is quantified, we are able to model *in vivo* behavior to quantify the effect of viscoelasticity. Through both experimentation and modeling, this study characterizes the viscoelastic behavior of bovine pulmonary tissue. Using five decaying exponential functions in the modified standard linear solid model, the various times at which the material responds to a strain can be evaluated. These time constants determine the time scale at which the viscoelasticity is most important. The results of this study will characterize viscoelasticity and determine the importance of its inclusion in constitutive models describing the mechanical behavior of pulmonary arterial tissue. A simplified model accounting for this time dependent behavior will also be introduced and verified.

CHAPTER II

II. Background

Biology Background

The pulmonary arteries are of particular biological importance, as they carry blood which is low in oxygen to the lungs, which in turn oxygenates the blood. The walls of these arteries are thick and the pressure is high as compared to the vessels in the rest of the body. The histological structure of arterial walls consists of four major components. The first of these components is the smooth muscle cells (SMCs). The SMCs are a living component of the wall, which under neural control, actively contract and expand causing a change in both the geometry and modulus of the vessel [1]. The smooth muscle cells are thought to be one of the viscoelastic components of the vessel [13].

The second component of the arterial wall is elastin, a rubber-like protein synthesized by the smooth muscle cells. Elastin in the arterial walls is present in its polymerized form, creating a fenestrated network of thin fibers. It has an elastic modulus on the order of MPa [14]. A second protein synthesized by SMCs is collagen. Collagen is inelastic, in that its modulus increases with increasing strain. The modulus is on the order of 10 MPa to a few hundred MPa [14]. Collagen is widely accepted as the main factor which causes nonlinear behavior of the tissue. It is also commonly understood that at low strains the collagen fibers are folded and do not contribute to the elastic properties until they are pulled taught. At this point the collagen fibers are able to bear a large portion of the stress. The fourth component of the artery is the ground substance. This is a gel-like, highly hydrated matrix and is usually not considered to contribute to the elastic properties of the wall [1].

These four components make up three layers, or tunicae, in the histological structure [2, 5]. This layered structure can be seen in Figure 1**.** The innermost layer is the intima, which consists of a monolayer of endothelial cells resting on a thin membrane. Although the intima is known to contribute to the flow control, the mechanical contribution of the endothelium to the wall is negligible. Thus, the contribution of the intima, as a whole, to the mechanical behavior or the arterial wall is commonly neglected [15].

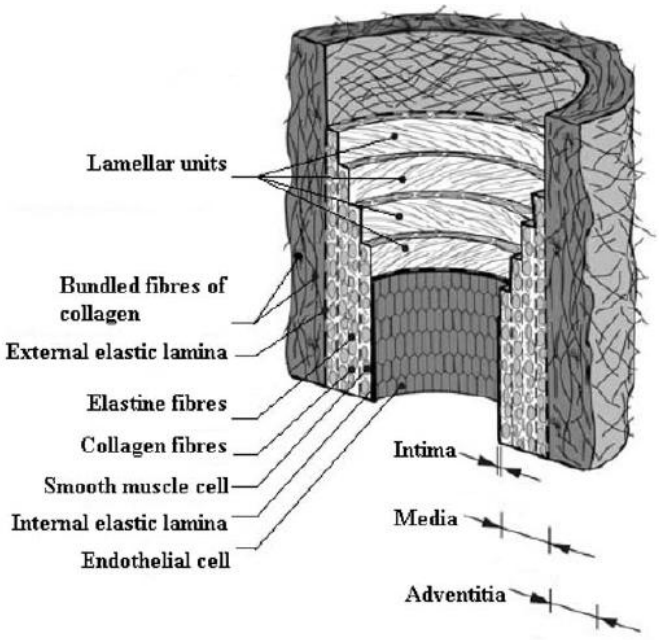

Figure 1. Diagrammatic scheme of the layered structure within the wall of an elastic artery adapted from [3].

The tunicae media is the middle and thickest layer of the arterial wall. It is separated from both the innermost and outermost layers by lamina consisting of elastin. The structure of the lamellae is able to change in order to minimize the radial stress gradient within the arterial wall [14, 16]. The outer layer (adventitia) of the vessel is mostly comprised of loose helical collagen fibers which are embedded within the ground substance. The adventitia consists of a small amount of elastin however SMCs are not present in the adventitia.

Material Properties

Arterial tissue is an orthotropic, highly nonlinear, composite solid made up of different constituent materials; thus, an effective constitutive model of the arterial wall requires understanding of the entire histology of the artery. First of all, arteries are subcategorized into two types: elastic and muscular. Elastic arteries are those located relatively close to the heart, and consequently have larger diameters. Conversely, muscular arteries are located at the periphery of the circulatory system. Since pulmonary arteries are located in close proximity to the heart, this work is limited to the study of elastic arteries. Each of these arterial types consists of the three separate layers: the intima, media, and adventitia [2, 5].

The intima consists of a single layer of endothelial cells which create a lining along the wall. In healthy tissues, the intima plays an insignificant role in terms of the solid mechanical properties. Of note however, is that the intima both thickens and stiffens with age, so it is possible that it could play a larger role in this case [3]. The media is made up of a complex network of both elastin and collagen fiber bundles. The orientation and configuration of the elastin and collagen fibrils, elastic laminae, and smooth muscles cells create a helix which gives the media high strength. This matrix also allows the media to resist loads in both the circumferential and longitudinal directions, each of which are described below. Due to all of this, the media is the most significant layer in terms of mechanical properties. The outermost layer of the artery tissue, the adventitia, primarily consists of fibroblasts and fibrocytes, which are cells that produce collagen and elastin respectively. The adventitia is much less stiff than is the media when in the assumed load-free configuration. However, under high pressures, the collagen fibers are engaged creating an extremely stiff structure in order to help resist rupture [3, 14].

Since under the physiological range of deformation arteries do not change their volume, they are assumed as incompressible. This assumption becomes very important because it allows the properties of three-dimensional materials can be determined through two-dimensional testing [3]. Uniaxial tests on arterial samples may provide basic information about the material but in order to sufficiently describe the anisotropic behavior of the tissue, biaxial testing must be done. The mechanical properties shown by this test are greatly dependent on both chemical and physical factors. These include a variety of parameters such as temperature and the pH of the bath. These among other dynamics reinforce the importance of noting such factors within the experimental data set. Also, the mechanical properties of the arterial walls change along the arterial tree, however the general behavior of the sample stays relatively consistent [3, 14].

Preconditioning

Mechanically characterizing biological soft tissues is extremely difficult due to the above mentioned material variables. Since biological tissues are both inhomogeneous and anisotropic, the material properties which are used to characterize the mechanical response are usually obtained from incredibly variable data. Not only do the tissues exhibit anisotropy, but they also have a spatially varying microstructure leading to even deviation of material data. These discrepancies are often attributed to the large natural variability of tissues, but in reality, neglecting the strain history-dependant viscoelastic response of the tissue can be the largest contributor to large data discrepancies [6].

During cyclic deformation, biological soft tissues demonstrate hysteresis, or memory effect, that is independent of rate over several decades of strain rate [17]. However, as the strain rate is increased in displacement controlled experiments, the overall stiffness of the tissue

increases [18]. On top of this, soft tissues show both stress relaxation and creep effects in response to constant displacement or load, respectively. Due to the strong time dependency of the tissue response, it is often very important to create a well specified loading history prior to any data collection [18].

All arterial tissues, and the vast majority of all biological soft tissues for that matter, exhibit strong, stress softening effects. This phenomenon occurs over the first few load cycles and eventually the material begins to produce a nearly repeatable stress strain curve [14]. For this reason, the initial curve is never used when characterizing mechanical properties of materials with memory [19]. This softening effect is very evident in Figure 2. A nonlinear stress-strain response is shown in all arterial tissue. The tissue is very flexible and highly deformable when small loads are applied. However, when the load (or pressure) is increased, the tissue exhibits an exponential stiffening rate caused by the engagement of the much stiffer collagen fibers [20].

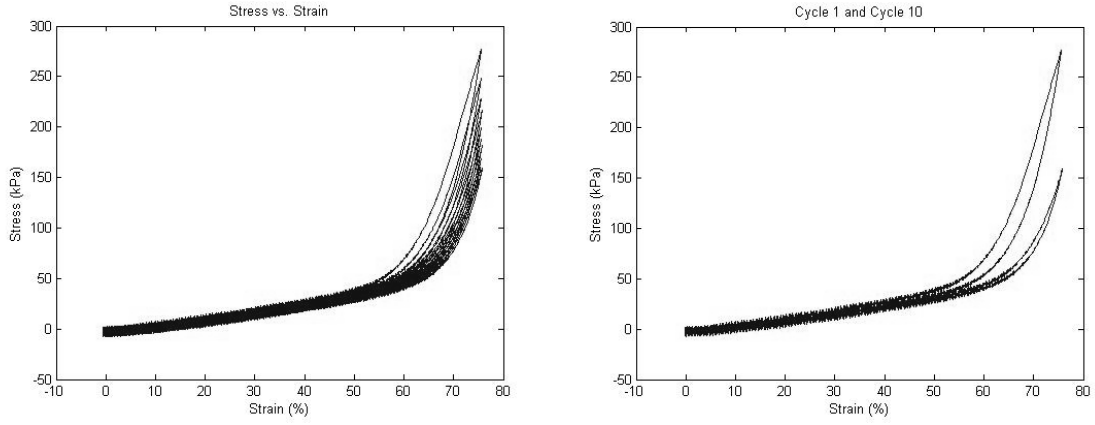

(A) (B)

Figure 2. Figure 2A shows the variation between the stress and strain responses of the same tissue over cycles 1 through 10. Figure 2B shows only cycle 1 and 10 of the preconditioning cycle. It can be observed that the loading and unloading path become increasingly similar until the curves become nearly repeatable.

Loading beyond the viscoelastic portion (when the curve changes from concave to convex) occurs in clinical treatments such as an angioplasty [1]. Deformation outside of the physiological range begins to bring about inelastic effects which can lead to drastic changes in material behavioral mechanics. This is caused due to a stress that is high enough to destroy various intermolecular bonds including the following: ligand-receptor interactions, proteoglycan interactions, and intermolecular bonds. In the case of altered material behavior, damage mechanics can be used to quantify the current behavior when compared to the non-stressed, virgin material properties [5, 14].

The occurrence of stress-softening is the reason for which in all research, some type of preconditioning is done to the sample. Figure 2 gives a visual representation of the effect of the so-called preconditioning through uniaxial test data. The plot on the left gives a good representation of how the material changes from cycle to cycle. It is easily noted that the first stretch reaches a much higher stress at the same level of strain. The plot to the right represents the first and last of the ten preconditioning cycles. Not only are the material properties much different, but perhaps more importantly, the tissue behaves as a history dependent material, returning along a much different stress-strain curve. The area between these curves is the hysteresis loop and shows that the material has ever changing properties with respect to time. Thus, the second cycle will start along the unloading path of the first which explains the shift of the curves to the right on the first plot. This example shows the assumed necessity of preconditioning arterial tissue in order to collect accurate data [14].

Preconditioning is obviously considered to be a very important component of biological tissue testing. It is reported that preconditioning provide benefits which consist of a known loading history and makes it possible to gain a both consistent and repeatable state for the period

of data recording [17]. Early studies on soft tissue properties showed that after about three preconditioning cycles, the tissue followed a consistent loading and unloading path, thus leading to repeatability throughout the test. Preconditioning has become standard test protocol when dealing with biological tissues for these aforementioned reasons. Both the stress-strain and stress-relaxation responses of biological tissues have been investigated using various combinations of max strain and strain rate. In most of these cases it is seen that the protocols involve cyclic preconditioning on the order of 3-30 cycles, which is somewhat dependant on the type of tissue sample being tested [18, 19]. It is also seen as commonplace for the studies to apply a maximum strain and a strain rate that correspond to the test which is being done. In tests that involve testing at various strain or strain rate combinations it is commonplace to have a preconditioning cycle which corresponds to each individual test [19].

Higher stress-strain responses can be seen in specimens which are preconditioned to a lower strain, suggesting that preconditioning strain magnitude does indeed affect the stress-strain response during the test [19]. As mentioned, it is common for studies to test biological samples under various combinations of strain and strain rate. Fiford and Bilston looked at spinal cord specimens which were tested under various conditions and the preconditioning which was performed corresponded to the strain and strain rate of the actual test [21]. However, the stress-strain data from these tests did not produce repeatable results; two curves taken under the same conditions did not overlap. It is very likely that this discrepancy is due to preconditioning the specimens to different strain magnitudes, therefore a common preconditioning strain magnitude should be used to obtain consistent data sets. Such a small issue can produce notable effects on both stress-strain and stress relaxation responses of these tissues. Notably the tissues in this analysis were spinal cords but it is presumed that the same principles could be applied when

considering preconditioning procedures in any biological tissue sample [19]. The discrepancy between preconditioning strain and mechanical property data achieved is shown below.

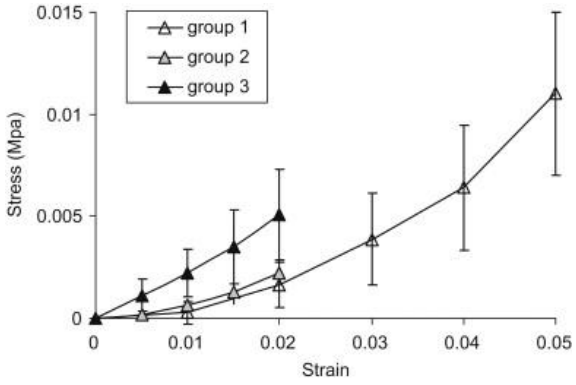

Figure 3. Stress–strain responses of spinal cords subjected to uniaxial strain of 2% (groups 2 and 3) and 5% (group1). While specimens of groups 1 and 2 were preconditioned to 5% strain, specimens of group 3 were preconditioned to a lower strain of 2% [19].

It has also been suggested to use repeated stress-relaxation cycles as a method of preconditioning. It had been assumed that both stress relaxation and creep experiments carried out from some generalized reference state would in themselves be repeatable, and thus generate accurate viscoelastic material constants. This procedure has been widely used, however it has also been shown that a repeatable stress relaxation curve cannot be obtained using conventional preconditioned state [6, 22]. The exact mechanisms of preconditioning remain unknown; however it is very likely that the cyclic loading at a specified strain induces structural rearrangement within the tissue. This allows the material to return to the same loading protocol [6].

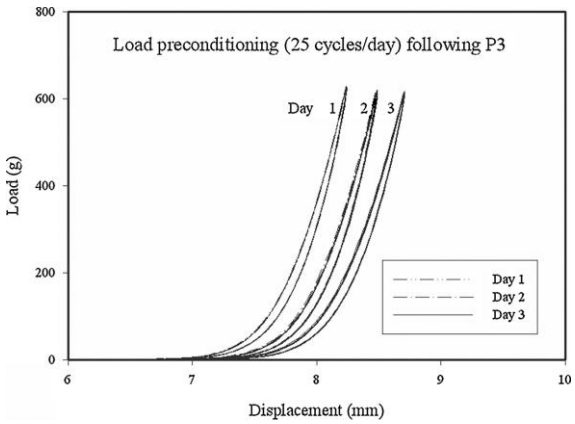

Figure 4. Load preconditioning curves from the same specimen shown in Fig. 6, after conclusion of the stress relaxation tests. Note that the 25 load preconditioning cycles plotted for each day are virtually identical, indicating that the specimen remains in a load-preconditioned state after each sequence of stress relaxation. There is evidence, however, of specimen lengthening (~6%) over the course of 3 days of testing [6].

The preconditioning procedure, coupled with the need to impose a reference load to ensure tissue tautness, changes the so called zero stress, zero strain state of the tissue. It is essential that this reference state be consistently represented as a part of modeling the subsequent soft tissue behavior, since it is a direct effecter of the stress and strain calculation. Typically, the stress and strain values are calculated using dimensions of the sample in a fully relaxed state or under a minute preload following the preconditioning procedure [18].

Preconditioning has even been questioned on being a valid procedure. This is due to the potential of variation both within and between different studies that the preconditioning strain may cause. Conversely, Gefen et al. [23] demonstrated that there is a large variation in biological tissue properties when preconditioning is not performed, thus making it seemingly preferable to perform a preconditioning procedure when examining the mechanical properties of these tissues [19]. Cheng et al. recommended that in future studies, that the preconditioning strain should be stated, and also performed to the highest strain of any test within that study. Secondly, if comparisons are made with another study, it would be useful to use the same

preconditioning strain as the comparison study for at least part of the test, resulting in much more meaningful data comparisons [19].

Analyzing mechanical properties of biological materials which exhibit viscoelastic behavior is extremely challenging. Viscous models are not universally acceptable and material testing protocols are far from standardized. For sake of statistical analysis, it is often beneficial to subject one sample specimen to sequential mechanical tests. This method eliminates the issue of material variability (which is a large issue in nearly all biological specimens) however there is an unknown effect of specimen memory. Preconditioning has been used to overcome these effects and although always mentioned as a necessary first step in soft tissue testing, the effects of intermediate preconditioning along with adequate recover times (or lack thereof) is not well understood [22].

Although preconditioning has become an accepted aspect of biological soft tissue mechanical testing, there is not a consistent preconditioning protocol [18, 19]. The effects of this preconditioning however seem to be qualitatively consistent in that multiple loading cycles lead to a repeatable data set [18].

Viscoelasticity

It is well known that the mechanical behavior of soft tissues is viscoelastic rather than elastic [7, 10, 11, 20, 24-38]. The biological functionality of the viscoelasticity is however not very clear. Understanding the changes in material properties of the arteries and the relationship with the viscoelastic properties should give a significant insight into the tissue's functional behavior [27, 28]. Blood vessels are typical biological soft tissues in that they exhibit highly nonlinear stress-strain relationships, are anisotropic, and have significant viscoelastic features.

Understanding the mechanical behavior, including viscoelastic relationship, is imperative when considering the vascular processes under both physiological and pathophysiologial conditions [38]. The pseudoelastic formulation, or investigation of the loading and unloading curves of the stress-strain response has already been widely used, however in order to do a more realistic analysis, the viscoelastic behavior of the arterial wall is becoming a much more relevant consideration [20, 34].

One hypothesis on the physiologic purpose of viscoelasticity is that it reduces the stresses and strains seen by the vessel walls, which could significantly affect the fatigue life of the artery. It is known that viscoelasticity in blood vessels helps reduce the wall stress and strain during a sudden mechanical load increase, as in hypertension. Even still, the complete functional role of viscoelasticity in blood vessels has not been fully understood [38]. In order to characterize the mechanical response of *in vitro* artery walls, uniaxial tensile experiments can be carried out. Biomechanical models are needed to classify arterial vessels both to further understand the biological functional behavior and to reduce the viscoelastic mismatch with arterial replacement. Stress relaxation tests allow the time dependant behavior of the tissues to be examined. In this case, biological soft tissues are not greatly affected by the strain rate of the loading ramp phase [28].

Looking at viscoelasticity from a mechanical perspective, it is possible that the energy dissipation produces heat which helps to maintain the homeostatic state of the tissues. Secondly, the hysteresis loop shown previously may filter out instantaneous loading changes, which could help in prevention of sudden mechanical failure. Viscoelasticity has not yet been related to the fatigue of arteries, despite its effect on this loading change. Based on current findings, Zhang et al. have hypothesized that the reduction of stress and strain due to the viscoelastistic arterial wall

property is beneficial in terms of artery fatigue life. Also, they hypothesize that in general, viscoelasticity is present in biological tissues to reduce fatigue failure. Their reasoning behind this assumption is based on the idea that fatigue should be significantly smaller in viscoelastic response when compared to a purely elastic response [38].

The arterial wall's slow, time-dependent uniaxial stress-relaxation decay can be characterized by implementing viscoelastic models. The decay can be described through weak power-law functions. Cariem et al. successfully applied the quasi-linear viscoelastic theory to modeling these responses, however accurate estimation of the relaxation parameters from the reduced relaxation is more difficult [28]. This method is used in order to reduce the mathematical complexity in characterizing the viscoelastic response in arteries along with other biological soft tissues [38]. Alternatively, the fractional calculus theory has been proposed to describe stress relaxation curves of healthy human aortas. In this study, stress relaxation measurements were taken at three incremental stress levels, as seen in Figure 5 [28].

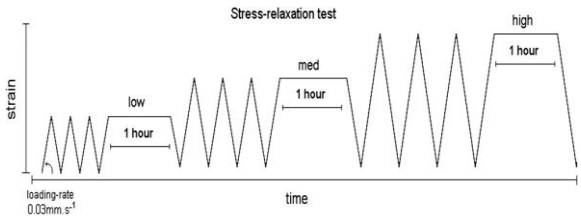

Figure 5. Schematic protocol with three stress levels: low (0.025 MPa), med (0.05 MPa) and high (0.1 MPa). Relaxation time = 1 hour. Loading rate during preconditioning ramps: 0.03 mm s^{-1} [28].

Using the data gathered from the protocol described above (Figure 5), Cariem et al. integrated a relaxation function, containing three parameters, into the quasi-linear viscoelastic theory to fit the experimental data. Their formulations were based on a modified Voigt model, which included a fractional element termed a spring-pot, which intermediates a standard spring

and dashpot [39]. This is similar to the dashpot except instead of a first order derivative, it is an alpha order derivative which is no longer limited to an integer value. This resulted in a very accurate stress relaxation prediction which shows a power-law decay matching the time course of all the stress relaxation experimental data [28, 39]. The accuracy of this prediction is shown in Figure 6.

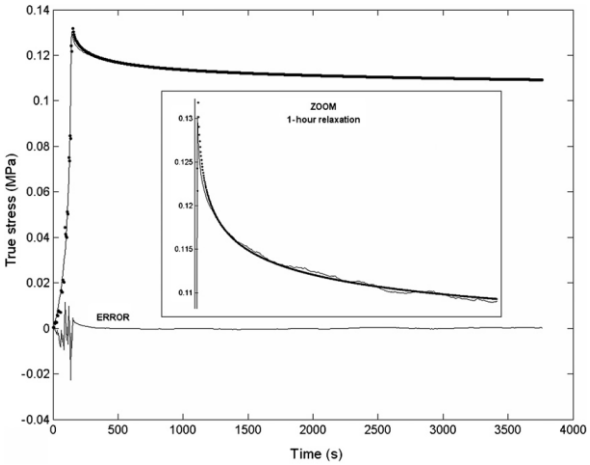

Figure 6. Ramp and stress relaxation example for specimen PH45 during stress level HIGH. Measured data in solid line and model fitting in dots. The difference (Error) between them is also drawn as a solid line. A magnified area of the peak and initial relaxation portions is shown the center of the figure. Image from Craiem [28].

Although there has been much consideration of viscoelasticity and its importance in the arterial vessel, the effect of this viscoelasticity under physiological loading conditions has yet to be quantified. In general, there is very little data on relaxation times of biological soft tissue, pulmonary arterial tissue in our case. In this work, we look to quantify the relaxation times of bovine, pulmonary tissue as well as delve into the significance of considering this viscoelastic effect when trying to accurately model pulmonary arteries under *in vivo* conditions.

Pressure-Diameter Relationship

Biomechical behavior of the artery needs to be further understood due to the widespread use of the balloon angioplasty to increase the lumen of an obstructed vessel through the use of an intravascular balloon catheter. The mechanisms of the balloon angioplasty as they relate to the mechanical behavior of arteries is however, very complicated. It does seem that the cells of bodily tissues tend toward a state which results in optimal stress and strain [40]. Very limited data has been available on vessel mechanics in this manner [31].

Histological tests have shown that the primary mechanisms comprise of overstretching the media and splitting of the intima [31]. This is relevant, since as stated earlier, the media and adventitia account for nearly all of the normal biomechanical behavior of vessels [14]. For this reason, studies on healthy arteries will help with the understanding of the overstretching of the vasculature.

Kang did a pressure-diameter analysis on common canine carotid arteries. The cannulated vessels were cyclically inflated and deflated from 0-200 mmHg at both 5 and 25 gram axial loads. As with other biological soft tissues, the specimens exhibited both hysteresis and a nonlinear pseudoelastic response. The arterial behavior at low pressures were nearly identical, however when the pressure was increased, the balloon induced specimens dilated considerably wider [41]. Figure 7 below gives a visual representation of this data. There is obviously a shift in the outer diameter of the vessel, as the control vessels do not expand to the same final diameter as the balloon-induced vessels. This means that there must be some type of weakening, or damage, to the blood vessel wall. Also of note, each of the vessels showed considerable stiffening with increased axial loads [31].

Current understanding suggests that pressure-diameter data are useful when qualitatively evaluating the behavior of normal and balloon-inflated vessels independently. Also, this data suggests that this can be done at various levels of axial loading [31].

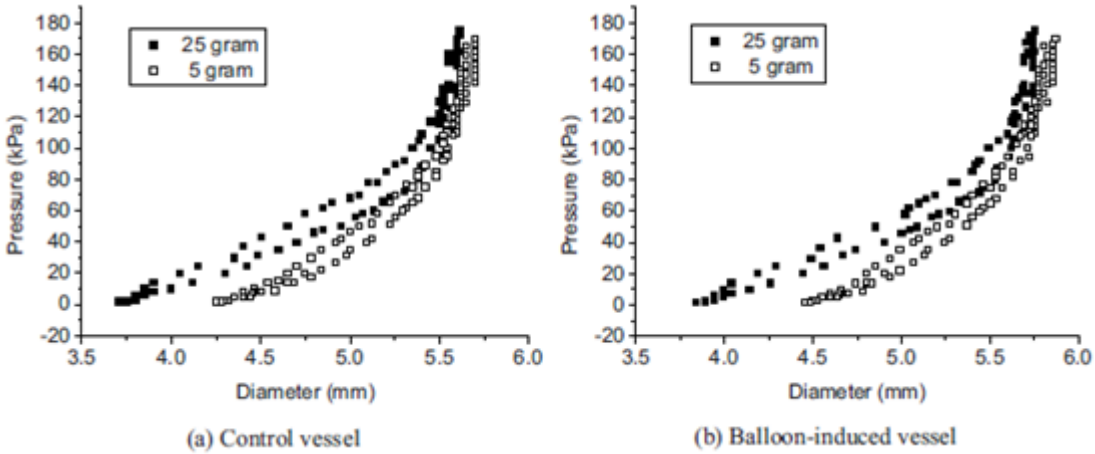

Figure 7. Comparison of vessel behavior (axial weights are 5 gram and 25 gram, respectively). Both the control and balloon-induced vessels stiffened with increased axial loads [31].

CHAPTER III

III. Experiments

Experimental Background

It has been proposed to use stress relaxation tests in order to examine the time dependent behavior of arterial tissue. These tests are able to be used since biological soft tissues are not greatly affected by the strain rate of the loading ramp phase, assuming a relatively quick loading rate [28]. Fitting the stress relaxation response to a stress relaxation function allows both the moduli and time constants to be determined for the arterial tissue [4, 8, 12]. This study investigates the quantitative, viscoelastic behavior of bovine pulmonary arteries through experimentation. Using five decaying exponential functions for a modified standard linear solid viscoelastic model, the mechanical parameters of the arterial tissue may be evaluated. The results of this study will determine the importance of considering viscoelasticity when modeling the stress behavior of arterial tissue. Also, the strain rate at which mechanical tests should be done in order to avoid strong relaxation effects will be quantified. Finally, a simplified model will be developed in order to easily account for the physiologic, viscoelastic behavior.

Materials and Methods

Sample Preparation

Bovine arterial samples for this study were obtained fresh (Arapahoe Meat Packing, Louisville, CO), within an hour of the animal's slaughter. Tubular, arterial sections from the main (MPA), right (RPA), and left (LPA) pulmonary arteries were removed at the same locations relative to the heart on each of the animals. Circumferential and longitudinal strips were excised from each respective arterial sample. The size of the strips varied between artery type since the

MPA has a much larger circumference and thickness than do either the RPA and LPA. A typical steady state length for the MPA was about 25 mm with a width and thickness of 7 mm and 4 mm respectively. Right and left pulmonary samples were on the order of 15 mm in length with a width of roughly 5 mm and thickness of 1.5 mm. Excised samples were immediately placed into a phosphate buffer solution and refrigerated to near freezing. A total of nine animals were used for this investigation. The bovine were roughly 12 months in age, weighing between 600 and 800 pounds.

Experimental Method

The mechanical tests on the pulmonary artery samples were conducted using an MTS Insight 2, with data acquisition via the TestWorks® MTS software. Samples were clamped into place using custom plastic grips and pulled taught. The entire setup was then enclosed within a plexiglass chamber for the duration of the tests in order to maintain a controlled environment. Phosphate buffer solution was poured into the environmental chamber and preheated to 37.1ºC in order to simulate *in vivo* conditions. The tissue sample was then preloaded to approximately 0.01N in order to remove all slack. At this point, the initial gauge length was recorded. Experimental data were taken at a rate of 100 points per second for the first 30 seconds and 10 per second for the remainder of the test.

A test method within the MTS software was programmed for our prescribed stress relaxation test. Each arterial sample was preconditioned for 10 cycles, at a strain equivalent to the relaxation test strain, prior to each relaxation test being performed. The sample was then ramped at 30% per second to the prescribed test strain. Constant test strain amplitudes of 35%, 45%, 55%, and 65% were applied respectively to the tissues, totaling four stress relaxation tests per sample. In order to minimize the chance of sample failure, tests were done in order of

increasing strain magnitude, starting with the 35% relaxation test. This is necessary since the maximum test strain (65%) is very close to the failure point of the material. For each relaxation test, the samples were held at each respective strain for a period of 1200 seconds in order to observe the stress relaxation behavior. This entire procedure was performed on each of the six bovine tissue samples (MPA, LPA, RPA in both longitudinal and circumferential directions) for a total of 24 relaxation tests per animal.

Data Fitting

For rate dependent materials, the modulus, $E(t)$, can be decomposed into

$$E(t) = E_0 + G(t) \tag{3.1}$$

Where E_0 is the equilibrium state modulus asymptote obtained as time approaches infinity, and $G(t)$ is the relaxation function describing the material relaxation characteristics. In this study, the aforementioned relaxation function was employed to determine the parameters describing the stress relaxation behavior. The model used was comprised of a spring and five Maxwell units, all in parallel. A decaying exponential equation (Prony series) was chosen as the reduced relaxation function for this model and is defined as in (3.1). The Prony series is a common form of constitutive equation used to describe relaxation behavior [4]. It was determined that five Maxwell branches were necessary in order to capture the strong, initial stress decay of the pulmonary artery.

$$G(t) = \sum_{i=1}^{5} E_i e^{\frac{-t}{\tau_i}} \tag{3.2}$$

E_i and τ_i are defined as positive constant values which can be determined through experimentation. Thus, the stress in the tissue is

$$\sigma(t) = \left[E_0 + G(t) \right] \varepsilon \tag{3.3}$$

The linear portion (E_0) describes the elastic stress behavior of the tissue while the relaxation function, $G(t)$, represents the time dependent, decaying nature of the stress response. The method of least squares was used within MATLAB to fit the experimental data to equation (3.3). This fit allowed the material constants for each of the data sets to be determined. As previously mentioned, it was here established that five Prony series were necessary in order to capture the strong initial stress relaxation response. This observation is the reason that 5 Maxwell elements were used in the aforementioned constitutive model.

Results

Typical Stress Response

Of the nine bovine, tissue samples from each artery, in each direction were obtained. A small number of tissue samples failed during testing so the corresponding data was left out. E arterial samples were preconditioned and elongated to 35%, 45%, 55%, and 65% respectively before undergoing the stress relaxation test. Figure 8 shows the normalized stress relaxation of the circumferential samples. Strains of 55% and 65% show a similar relaxation trend while the 35% and 45% strained samples showed a lower degree of relaxation, especially in the first 300 seconds. Past that point, the decaying rate slowed to a similar magnitude for each of the strain cases. The 55% and 65% samples decayed to a normalized stress rate of less than 0.7 while the 35% and 45% strained samples decayed to a normalized stress of about 0.8. These trends were common in both the circumferential and longitudinal directions. The data in Figure 8 is an average of all bovine arterial data. The right plot shows the normalized stress relaxation behavior of the longitudinal samples throughout the same strain regime. Decaying trends are similar to those seen in the circumferential directions. As the test strain was increased, the relaxation decay through the first 300 seconds increased.

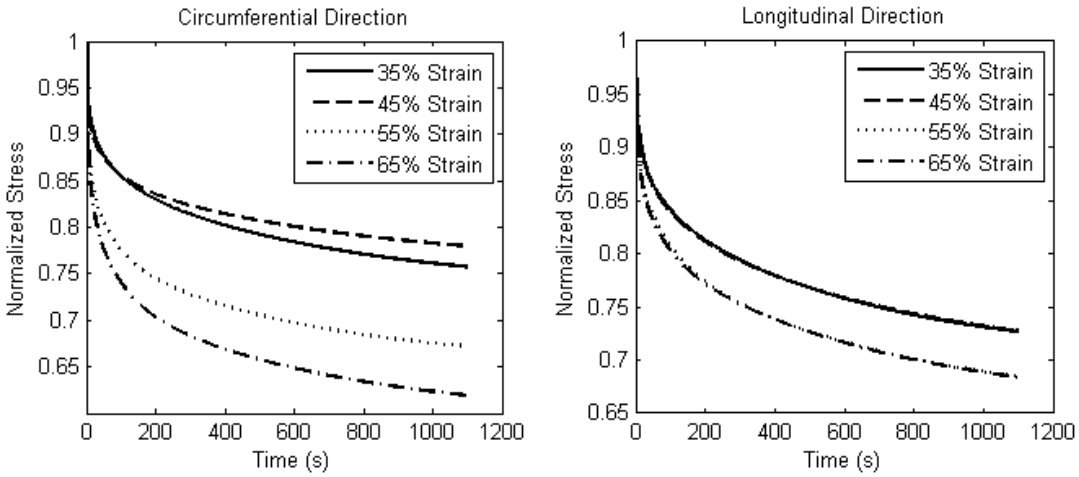

Figure 8. Normalized stress relaxation response for the circumferential and longitudinal directions. The observed stress for the 65% strain case falls to below 70% of the initial stress as time approaches 1200 seconds. It is seen that even with low constant strain, the final stress response is less than 80% of original. The rate at which the stress decreases becomes linear at approximately 300 seconds in all of the cases.

In order to model the stress relaxation behavior, the experimental curve was fit to a Prony series model. Initially, it was thought that a 2 term Prony series would be sufficient in fitting the experimental data. However, as shown in Figure 9, in order to capture the strong initial stress decay, it was necessary to include 5 terms in the Prony series (as shown in (3.2)).

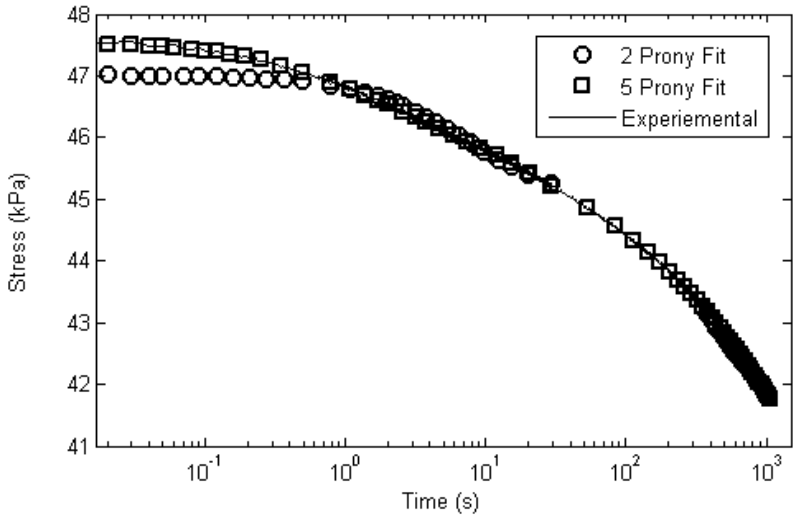

Figure 9. Sample curve fit of the Prony series model to the experimental relaxation data. Initially, the data was fit to a two Prony series model however it was found that five Prony series were necessary to capture the strong initial relaxation of the tissue.

Grouped Stress Response

For the first analysis, the individual data sets (for both tissue location and direction) were simply pooled together in order to show the overall trends. It can be seen from Figure 10 that the time constants followed a fairly normal data curve. In total, 184 measured time constants were combined to form this set.

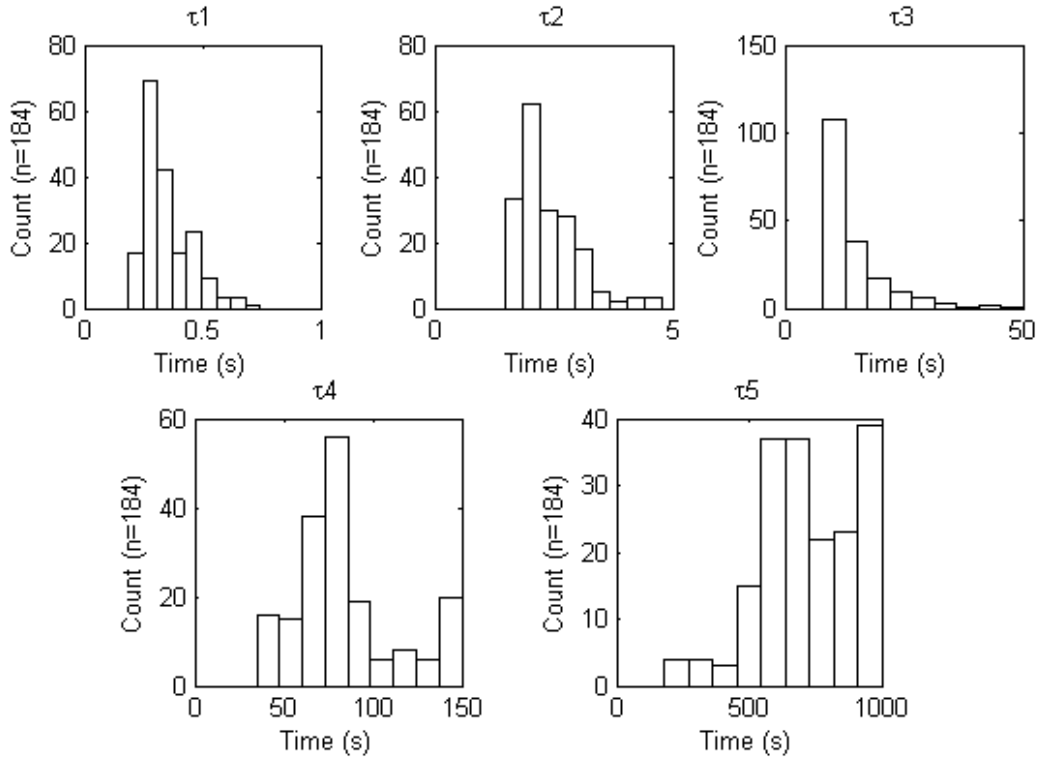

Figure 10. Histograms of the pooled time constants for all of the gathered data. The data follows a relatively normal distribution curve. No major trends were observed between the tissue locations (MPA, RPA, LPA) nor the direction (circumferential, longitudinal).

The time constants were relatively consistent throughout the strain regime for each of the tissue samples. Table 1 below plots each of the average relaxation times for each respective tissue and direction. The relaxation times were very similar between the circumferential and longitudinal directions. This is true for the initial relaxation constant (0.3 - 0.4 seconds) all the way to the longest time constant (~700 - 800 seconds). Similarly, the time constants change only minimally between different tissues (MPA, RPA, LPA).

Table 1. Average and standard deviation of all time constants as determined by Prony series curve fitting.

MPA		**τ1**	**τ2**	**τ3**	**τ4**	**τ5**
Circ.	*Avg.*	**0.392**	**2.489**	**16.064**	**86.112**	**803.503**
	Stdv.	0.082	0.473	8.901	33.3545	234.913
Long.	*Avg.*	**0.408**	**2.630**	**14.827**	**83.842**	**692.722**
	Stdv.	0.101	0.753	5.955	39.386	239.192
RPA						
Circ.	*Avg.*	**0.296**	**2.183**	**14.307**	**78.673**	**666.709**
	Stdv.	0.069	0.499	7.752	24.001	154.996
Long.	*Avg.*	**0.324**	**2.305**	**14.593**	**87.575**	**696.701**
	Stdv.	0.119	0.784	8.134	29.521	153.156
LPA						
Circ.	*Avg.*	**0.316**	**2.269**	**12.840**	**84.202**	**738.649**
	Stdv.	0.073	0.565	5.108	27.015	169.306
Long.	*Avg.*	**0.369**	**2.440**	**13.271**	**84.207**	**774.888**
	Stdv.	0.094	0.679	6.630	29.554	158.003

The moduli determined from fitting the 5 term Prony series is shown in Figure 11. In general, for all of the tissues, the modulus increased with larger time constants. This suggests that the time constants corresponding to a smaller time scale are less influential on the overall mechanical behavior. Conversely, the larger moduli would be assumed to be more relevant, assuming that their respective time scale is reached.

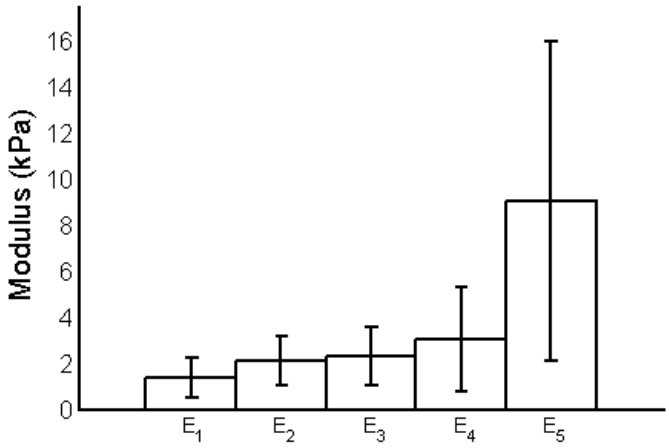

Figure 11. Plot of the grouped branch moduli with standard deviations. The moduli were found by fitting the 5 term Prony series (Eq. 2). The moduli corresponding to the fastest time constants are generally lower in magnitude than are the moduli related to the slower time constants.

The time constants determined from curve fitting were also plotted, as shown in Figure 12. The standard deviations for these time constants were relatively low, suggesting that there is little difference when comparing either tissue location or tissue direction. Interestingly, the time constants follow the logarithmic scale very well.

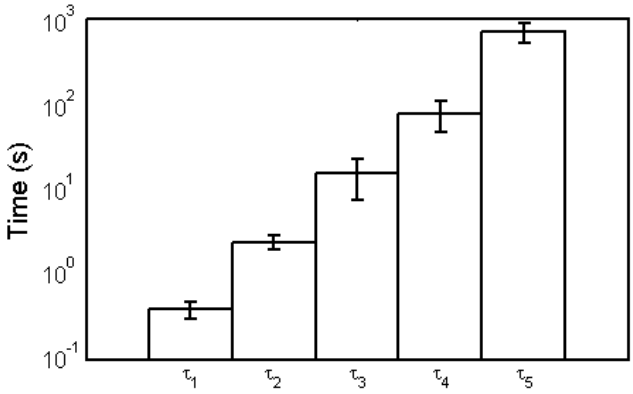

Figure 12. Semi-log scale plot of the grouped relaxation times with standard deviations. The standard deviations are relatively small suggesting that the time scale my not significantly differ between either tissue location or tissue direction.

Effects of Strain Levels

The strain level used for the relaxation test was not shown to have a significant effect on the observed relaxation curve parameters. Figure 13 presents the average values for the moduli and standard deviations for the main pulmonary artery data in the circumferential direction. Similarly, Figure 14 shows the average time constant values for the same data set. For the sake of simplicity, it was determined to present only the circumferential, MPA data set since it is the most physiologically significant for this discussion. The main pulmonary artery is closest to the heart and the circumferential direction should be more relevant to pulsatile blood flow [14].

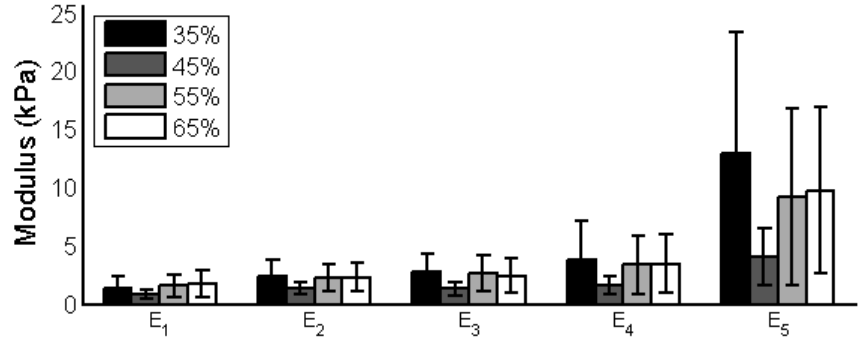

Figure 13. Plots of the average moduli in relation to the test strain. The data set chosen for these plots was that from the MPA in the circumferential direction. It can be seen from the plots that there is no strong correlation between the observed moduli and the strain at which the test was performed.

The moduli are again shown to increase with relaxation time. The modulus for the longest relaxation time is much greater than is the moduli of the fastest relaxation time. There is no significant difference between the test strain and the measured modulus.

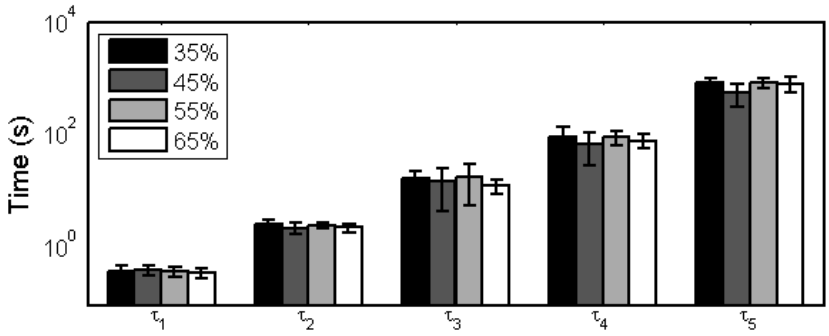

Figure 14. Plots of the average time constants as a function of test strain. The data set chosen for these plots was that from the MPA in the circumferential direction. It can be seen from the plots that there is no correlation between the observed relaxation times and the strain at which the test was performed.

Effects of Locations

Now, we will again consider each of the tissue locations (MPA, RPA, LPA). Since Figure 13 and Figure 14 have shown that test strain does not have a large effect on either the measured moduli or the measured time constants, we will consider only the 55% test strain for this section. The moduli follow the same trends, in that the slower relaxation times correspond to a higher modulus. The difference however, lies in the moduli of each respective direction. In

general, it seems as though the left pulmonary artery has the highest moduli followed by the right and main pulmonary arteries respectively. This is shown in Figure 15.

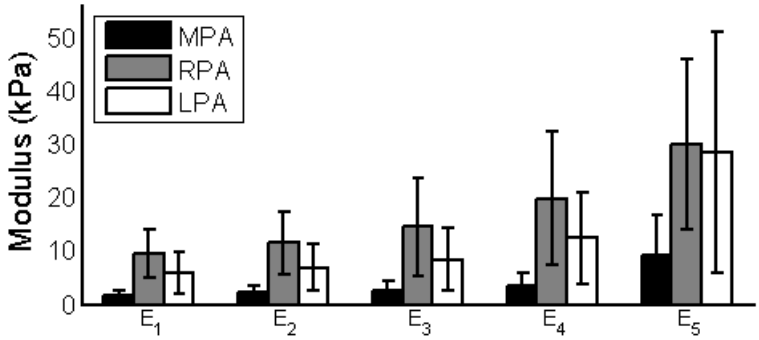

Figure 15. Plots of the average moduli in relation to the tissue direction. The data set chosen for these plots was that from the circumferential direction taken at 55% strain. It seems as though the RPA produces the highest moduli followed by the LPA and MPA respectively.

Unlike the differing moduli, the relaxation times seem to be very consistent regardless of tissue location. Again, the time constants increase in a very logarithmic fashion and no significant difference is seen between the MPA, RPA, or LPA respectively.

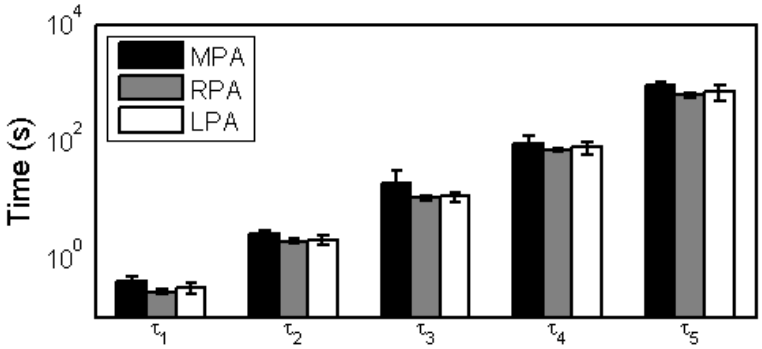

Figure 16. Plot of time constant data for the MPA, RPA, and LPA in the circumferential direction at 55% test strain. As expected, there is little variation in the relaxation time scale between the three tissue types.

Effects of Directions

The last comparison looks at the effect of the direction on the observed parameters. In this relation we again consider only the main pulmonary artery at 55% test strain. The moduli

followed the same trend seen in each of the other comparisons, where the time constants have a higher corresponding modulus than do the fastest relaxation times. From Figure 17, we can see that the direction did not seem to greatly affect the observed modulus, although in each case the circumferential direction did seem to be slightly stiffer, agreeing with claims by Hozapfel [20].

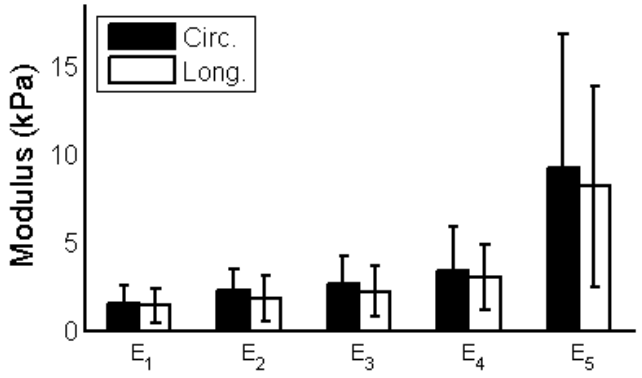

Figure 17. Plots of the average moduli in relation to the test strain. The data set chosen for these plots was that from the MPA at 55% test strain. It can be seen from the plots that there is no strong correlation between the observed moduli and the direction of the tissue, although the circumferential direction does provide slightly stiffer average moduli in all cases.

As in each of the other comparisons, there is no correlation between the direction and the observed relaxation times. These results are shown in Figure 18.

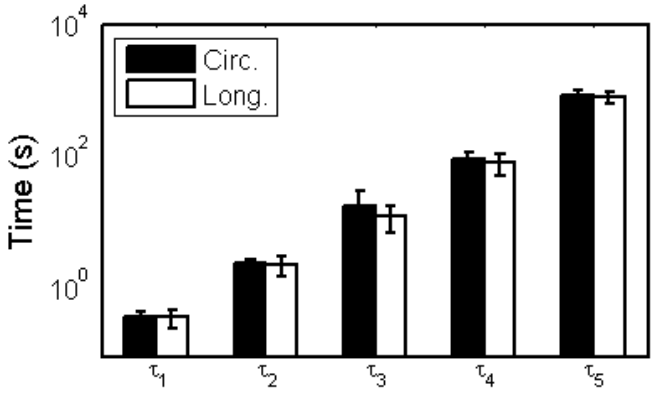

Figure 18. Plots of the average time constants as a function of test strain. The data set chosen for these plots was that from the MPA at 55% test strain. It can be seen from the plots that there is no correlation between the observed relaxation times and the strain at which the test was performed.

Experimental Results

The initial study investigated the time dependence of bovine arteries as well as the ability of the reduced relaxation function to accurately describe the stress relaxation phenomena. The two different sample directions (circumferential and longitudinal) were considered due to the difference in fiber orientation [5] in order to determine the directional effect of viscoelastic properties. It has been shown that in skin tissue, fiber orientation seems to affect the stress relaxation behavior of the samples; the regular fiber realignment process can only occur when a mechanical load is exerted along a particular fiber direction [8]. In our study, a significant difference in the decaying rate over the first 300 seconds was not observed when comparing circumferential to longitudinal directions. Also of note, the summation of the five moduli parameters was found to be slightly larger in the circumferential direction than in the longitudinal direction. Physiologically, this result seems to make sense as the *in vivo* artery experiences much more force in the radial direction when compared to the longitudinal direction. This claim agrees with the literature as it has been previously shown that arterial tissue is stiffer in the circumferential than in the longitudinal direction [3, 14]. Stress caused by tension along the axis of the artery should be relatively small when compared to the radial stress from pulsatile blood pressures. This phenomenon was observed in each of the tissue locations (MPA, RPA, and LPA).

The relaxation times of the material did not differ greatly between either sample location or direction. Although all of the respective groups (MPA, RPA, LPA) were not shown to be equivalent by the two sample t-test, the magnitude of the difference was very minute. It was observed that the relaxation times showed little variation between the circumferential and longitudinal directions. The group averages of each of the three longest relaxation times lied within 3.5% between circumferential and longitudinal. Similarly, each of the two short time

constants was within 10% between circumferential and longitudinal. All of the average time constants did however increase slightly from the circumferential to longitudinal directions, although minimally. This result implies that there is little or no difference in time dependency between the circumferential and longitudinal directions,. Perhaps further research need be done on this as it is outside the scope of the current study. The experimental time constant data can be seen in the comparisons presented in the results section. Although the data was not shown to be similar in the t-test ($p>0.05$), the standard deviation from the sample means overlapped between both tissue type and direction for each of the respective time constants. Also of note, the test strain did not seem to have any effect on any of the relaxation times achieved from the reduced relaxation curve data fit. However, as seen in Error! Reference source not found., the normalized magnitude of the relaxation decay did increase with increasing strain in both of the tested directions. Experimental results did show the relaxation rate approaching steady state after 300 seconds for all of the samples, verifying the time dependent nature of the arterial tissue. These results are similar to those found by Liu for the relaxation of porcine skin tissue [8].

Similarly, the test strain did not have a large effect on the modulus parameters. As expected, the equilibrium static modulus, E_0, also remained fairly constant with increasing strain. Only at high strains (65%) did the relationship seem to deviate, in which case the material is very close to its strain of yielding. This resultant is sensible as this portion of the model describes the elastic (spring) response of the tissue, which is assumed to be linear. The remaining moduli did not seem to be influenced by the test strain. As shown in the comparisons in section 3, the measured moduli were relatively consistent with respect to both tissue direction and tissue location as well. The only noteworthy difference is shown in Figure 15. The moduli of the RPA seem to be substantially larger for all time constants than both the LPA and MPA. Similarly, the

moduli of the LPA are stiffer than each of the MPA. Perhaps this is due to the smaller dimensions of both the RPA and LPA when compared to the MPA.

The normalized stress plots seen in Error! Reference source not found. show that there is a very strong decline in the magnitude of the stress response over the observed time period. Even at low test strains, the stress response decreased over 20 percent. At more the extreme case of 65 percent test strain, the stress response decreased to nearly 65 percent of its original value. In general, with increasing test strain, the percent decrease of the normalized stress response grew. In the case of the longitudinal direction (Error! Reference source not found.), there was a decrease in normalized stress response throughout the strain regime. Strains of 35 and 45% produced similar normalized responses while the normalized response of both 55 and 65% strains were significantly lower. There were similar results seen in the circumferential direction, shown in Error! Reference source not found.. There was no significant difference between the circumferential and longitudinal normalized relaxation curves.

The strong relaxation, especially at high strains, suggests that static data might not accurately describe stress magnitudes. For example, static pressure-diameter data may not produce an accurate representation of the true vessel pressure-diameter curve. This would be the case if, in its *in vivo* state, the tissue is not entirely relaxed. On the other hand, if the tissue does fully relax under biological loading, stress relaxation would have to be considered when developing mechanical test methods. After 1 second of relaxation, it was observed that there was an average decrease of 2% in the magnitude of the stress. After 6 seconds this relaxation resulted in about an 8% decrease in observed stress. This data suggests that the loading ramp phase for a uniaxial test should take place as quickly as possible in order to reduce the effects of relaxation, agreeing with the statements of Craiem [28].

CHAPTER IV

IV. Modeling

Novel Model from Stress Relaxation Experiment

This initial investigation has shown that arterial tissues do indeed exhibit viscoelastic behavior. Now we will focus on determining what effect this viscoelastic nature has on the ultimate mechanical response of an *in vivo*, pulmonary artery. Knowing this, we can make a judgment on the importance of considering the viscoelastic nature, both when testing and modeling pulmonary tissue. For the simulation, the frequency of the heart rate oscillation for bovine is assumed to be approximately 95 beats per minute. Using this information, along with the time constants from Table 2, we can model how this time dependency affects the stress behavior of the artery under these prescribed, physiologic conditions. Taking data from Table 1 and 2 for 35% strain, the stress-strain behavior can be predicted for each branch and then summed using the Boltzmann superposition principle.

The Boltzmann integral can be applied in order to describe the stress behavior of a Maxwell element with a known strain behavior. For this case, the Boltzmann integral is defined as:

$$\sigma_i(t) = E_i \int_{-\infty}^{\infty} e^{-\frac{t-s}{\tau_i}} \dot{\varepsilon} ds \tag{4.1}$$

where $\sigma_i(t)$ is the stress at time t. E_i and τ_i are defined as the modulus and time constant for the ith Maxwell branch. Finally $\dot{\varepsilon}$ is defined as the change in applied strain. For this case, the strain is initially equal to zero so the integral bounds can be taken as follows:

$$\sigma_i(t) = E_i \int_{0}^{t} e^{-\frac{t-s}{\tau_i}} \dot{\varepsilon} ds \tag{4.2}$$

The prescribed strain input used in this simulation is comprised of an initial, linear, loading portion followed by a cyclic load. The general strain is applied as in (4.3). For continuity in the function, (4.4) must be satisfied.

$$\varepsilon(s)=\begin{cases} At,\ t<t_1 \\ (At_1-A_1)+A_1\cos\left(h(t-t_1)\right),\ t\geq t_1 \end{cases} \tag{4.3}$$

$$At_1=\varepsilon_0+A_1\cos\left(h(t-t_1)\right)=\varepsilon_0+A_1 \tag{4.4}$$

The total strain after t_1 can thus be described and simplified as follows:

$$\varepsilon(t)=\varepsilon_0(t)+\Delta\varepsilon(t) \tag{4.5}$$

$$\varepsilon_0(t)=\left(At_1-A_1\right) \tag{4.6}$$

$$\Delta\varepsilon(t)=A_1\cos\left(h(t-t_1)\right) \tag{4.7}$$

Combining (4.3) with (4.4) and taking the derivative we arrive at the change in strain

$$\dot{\varepsilon}(s)=\begin{cases} A,\ t<t_1 \\ -A_1h\sin\left(h(t-t_1)\right),\ t\geq t_1 \end{cases} \tag{4.8}$$

The stress then becomes the summation of two functions. The first is the response to the linear, loading phase where $t<t_1$. The second function describes the cyclic strain, or when $t\geq t_1$. This produces the following result.

$$\sigma_i(t)=\sigma_i^{linear}(t)+\sigma_i^{cyclic}(t) \tag{4.9}$$

Applying the step function in (4.8) to (4.2) we reveal the stress response for both the linear and cyclic portions.

$$\sigma_i^{linear}(t)=E_i\int_0^t Ae^{-\frac{t-s}{\tau_i}}ds \tag{4.10}$$

$$\sigma_i^{cyclic}(t)=E_i\int_0^{t_1} Ae^{-\frac{t-s}{\tau_i}}ds+E_i\int_{t_1}^{t}-A_1h\sin\left(h(s-t_1)\right)e^{-\frac{t-s}{\tau_i}}ds \tag{4.11}$$

Integrating (4.10) and (4.11) the following results are achieved, respectively.

$$\sigma_i^{linear}(t) = AE_i\tau_i\left(1-e^{\frac{-t}{\tau_i}}\right) \tag{4.12}$$

$$\begin{aligned}&\sigma_i^{cyclic}(t)\\&= E_i\left[A\tau_i e^{\frac{-t}{\tau_i}}\left(e^{\frac{t_1}{\tau_i}}-1\right)-\frac{A_1 h\tau_i}{1+h^2{\tau_i}^2}\left[h\tau_i e^{\frac{t_i-t}{\tau_i}}-h\tau_i\cos\left(h\left(t_1-t\right)\right)-\sin\left(h\left(t_1-t\right)\right)\right]\right]\end{aligned} \tag{4.13}$$

Placing (4.12) and (4.13) back into (4.9) and plugging in the boundary conditions, the total stress in the Maxwell element over the prescribed strain regime can be formulated.

$$\begin{aligned}&\sigma_i(t) = AE_i\tau_i\left[1-e^{\frac{-t}{\tau_i}}\right]_0^{t_1}\\&+E_i\left[A\tau_i e^{\frac{-t}{\tau_i}}\left(e^{\frac{t_1}{\tau_i}}-1\right)-\frac{A_1 h\tau_i}{1+h^2{\tau_i}^2}\left[h\tau_i e^{\frac{t_i-t}{\tau_i}}-h\tau_i\cos\left(h\left(t_1-t\right)\right)-\sin\left(h\left(t_1-t\right)\right)\right]\right]_{t_1}^{t}\end{aligned} \tag{4.14}$$

Assuming that t_1 is small, the initial term can be dropped in order to observe the behavior as t becomes large. Applying the boundary conditions and simplifying the remaining terms, we arrive at the following:

$$\sigma_i(t) = E_i\left[\frac{A_1 h\tau_i}{1+h^2{\tau_i}^2}\left[h\tau_i\cos\left(h\left(t_1-t\right)\right)+\sin\left(h\left(t_1-t\right)\right)\right]\right] \tag{4.15}$$

Since the sine and cosine terms are always between negative one and one, assuming that $h\tau_i$ is substantially larger than one, the sine term becomes negligible.

$$\sigma_i(t) = E_i\left[\frac{A_1 h^2{\tau_i}^2}{1+h^2{\tau_i}^2}\left[\cos\left(h\left(t_1-t\right)\right)\right]\right] \tag{4.16}$$

Assuming that $h^2{\tau_i}^2$ is substantially larger than one, (4.16) reduces to the final, simplified stress equation for the stress in one Maxwell element as t becomes very large.

$$\sigma_i(t) = E_i A_1\left[\cos\left(h\left(t_1-t\right)\right)\right] \tag{4.17}$$

This final stress equation is a simplified stress response for one Maxwell element undergoing a cyclic strain (as described by (4.3)), similar to what would be seen by the *in vivo* pulmonary vasculature. Using the Boltzmann superposition principle, this result can be applied to each of the five Maxwell branches in the model and summed to formulate the total viscoelastic stress response. This viscoelastic stress can then be added to the elastic stress to produce the total stress response of the model to a cyclic strain input.

$$\sigma(t) = \sigma_0(t) + \sum_{i=1}^{5} \sigma_i(t) \tag{4.18}$$

In (4.18), the linear stress behavior is described as:

$$\sigma_0(t) = E_o \varepsilon(t) \tag{4.19}$$

Combining (4.5) and (4.18) we can achieve the following equation describing the total stress response.

$$\sigma(t) = E_o[\varepsilon_0(t) + \Delta\varepsilon] + \Delta\varepsilon\left(\sum E_i\right) \tag{4.20}$$

In our case, this simple model was tailored to mimic an *in vivo*, bovine, main pulmonary artery. A typical, healthy, bovine MPA sees strains that cycle between about 20% and 40%. Using (4.3), the following equation was developed to describe the strain input.

$$\varepsilon(s) = \begin{cases} \dfrac{4}{30}t, \; t < 3 \\ 0.3 + 0.1\cos\left(10(t-3)\right), \; t \geq 3 \end{cases} \tag{4.21}$$

Using this strain input, the artery undergoes a quick linear loading phase followed by a cyclic, wave strain. This gives a simplification of the change in the diameter of the vessel due to the heart beat. The heart beat is approximately 95 beats per minute in this case, which is appropriate for the bovine considered in this study. Using these input parameters, the stress response (4.17) becomes:

$$\sigma_i(t) = E_i\left[\frac{1}{10}\left(\cos\left(10t - 30\right)\right)\right] \tag{4.22}$$

Using Matlab, (4.21) was applied to (4.2) in order to simulate the stress-strain response as a function of time. This result was then compared against the simplified, final stress response shown in (4.22). These results can be seen in Figure 19**.**

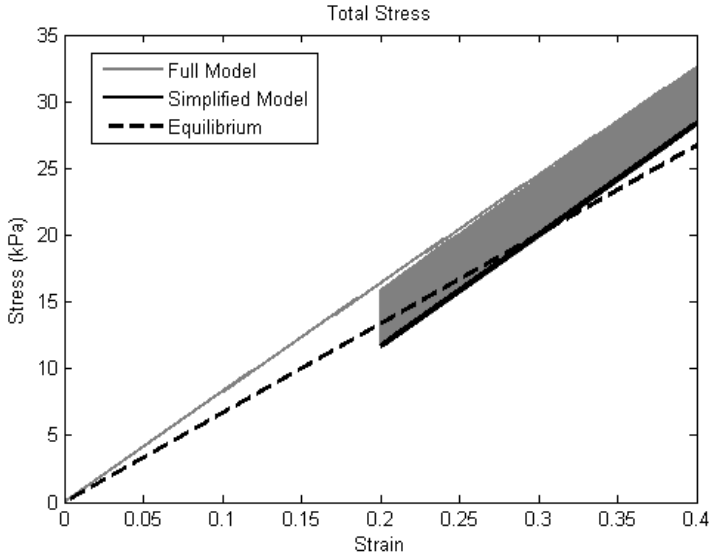

Figure 19. Matlab simulation of the stress-strain response using the cyclic strain input (with a linear initial loading ramp) described in Equation (4.21). The simulation was run until t = 10^5 seconds. This result is compared against Equation (4.22), which is the simplification for the stress response to the same input as t approaches infinity.

The simulation was done assuming the same material model as previously applied: five Maxwell elements (all in parallel) in parallel with a spring element. The model input parameters were taken from the experimental bovine data for the main pulmonary artery at 35% strain. These input parameters can be seen in Table 2**.** The breakdown of the stress vs. strain response in each Maxwell element is shown in Figure 20**.**

Table 2. Matlab model input parameters.

E1	*1.18 kPa*	*modulus of first Maxwell element*

E2	*1.92 kPa*	*modulus of second Maxwell element*
E3	*2.14 kPa*	*modulus for third Maxwell element*
E4	*2.80 kPa*	*modulus of forth Maxwell element*
E5	*8.55 kPa*	*modulus of fifth Maxwell element*
E0	*66.82 kPa*	*modulus of spring element*
τ1	*0.39 s*	*time constant of first Maxwell element*
τ2	*2.49 s*	*time constant of second Maxwell element*
τ3	*16.06s*	*time constant of third Maxwell element*
τ4	*86.11 s*	*time constant of forth Maxwell element*
τ5	*803.50 s*	*time constant of fifth Maxwell element*

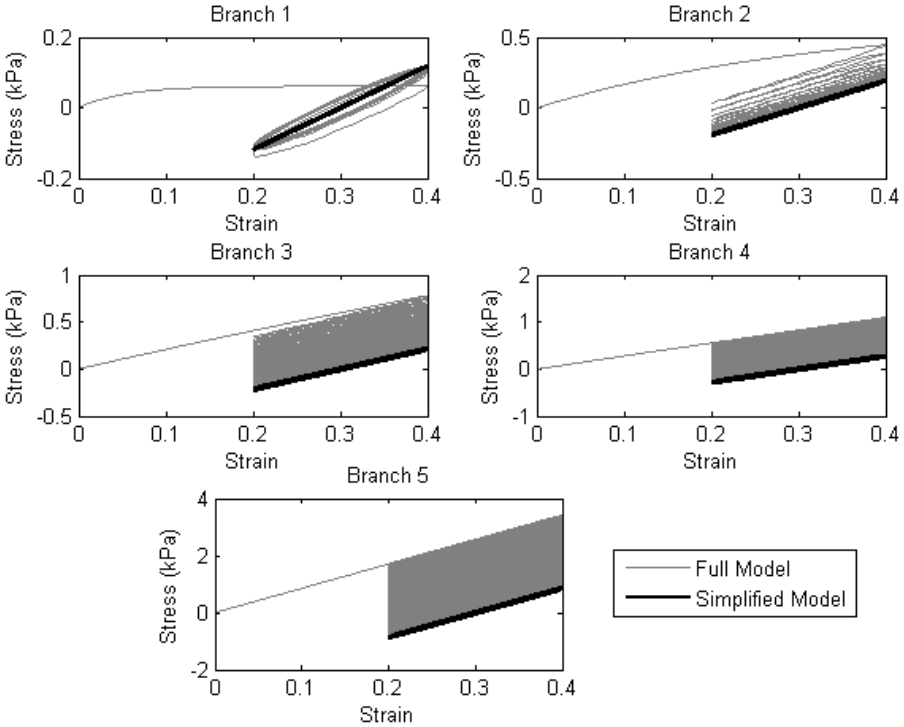

Figure 20. Matlab model predicted stress-strain response for each individual Maxwell element. The stress decreases to equilibrium as time becomes large. It can also be seen that the predicted response from Equation (4.22) fits very well for each of the individual branches.

From Figure 20 we can see that the prediction from Equation (4.22) fits out model very well. The only deviation is in the first element where the approximation is linear while the actual

response is a small loop. However, the slope is equivalent and due to the small magnitudes of the values in element one, the differences caused by the loop become minute when the total stress response is observed in Figure 19**.**

The results of this simulation show that although the viscoelastic properties of bovine vascular tissue are quite pronounced, a very simple constitutive model can be applied to accurately describe the *in vivo* behavior. This success of this model is linked to both its ability to accurately predict the *in vivo* stress-strain response and its overall simplicity.

Our findings agreed with the results of Grashow et al. They found that the mitral valve anterior leaflet exhibited significant stress relaxation. They did however see that there was negligible creep seen over a 3 hour test [7]. Cox et al. examined the viscoelastic properties *in vitro* pulmonary of canine. Measurements of force in response to sinusoidal perturbations were made over the frequency range of 0.002 Hz to 10 Hz. It was found that most of the frequency dependence of the dynamic modulus occurred on the lower end of this range, under 0.1 Hz. This viscoelasticity is thought to be a representation of the smooth muscle contribution in the wall of the arteries [13]. Our model was thus modified by adding a smooth muscle term to (3.2). The smooth muscle term (σ_s) is described as follows.

$$\sigma_s = E_s e^{\frac{-t}{\tau_s}} \tag{4.23}$$

The relaxation time of the smooth muscle term was taken to be equivalent to the fastest of the above relaxation times (τ_1 = 0.39s). In order to determine the possible contribution of the smooth muscle, the modulus, E_s, was varied in terms of E_0. Initially E_s was taken to be 5% of E_0, and then incrementally increased to 10, 20, and 30% of E_0 respectively. The ultimate tissue response with the incorporated smooth muscle contribution is shown in Figure 21.

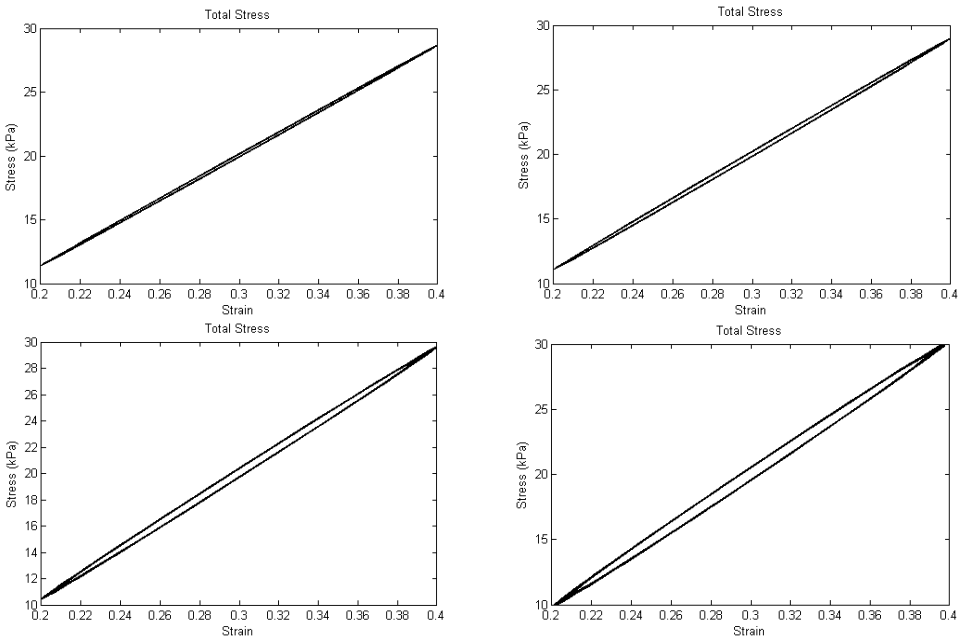

Figure 21. Matlab model ultimate predicted stress-strain response with added smooth muscle branch. The time constants for the smooth muscle effects was equal to τ_1 and the smooth muscle branch modulus was varied between 5, 10, 20, and 30% strain from top left to bottom right respectively. With a smaller modulus, the hysteresis loop is much smaller when compared to larger values of E_s.

These model results show that as expected, a larger modulus on the fastest time constant causes a hysteresis loop to form in the ultimate stress-strain response.

Finite Element Verification

It was felt necessary to validate the experimental results found in the previous section through the use of finite element modeling. *In vivo*, the pulmonary artery is experiencing a pressure-diameter relationship as opposed to the simplified, uniaxial stress-strain relationship suggested above. Although our uniaxial results are as expected, and agree fairly well with previous research [8, 11], a simple, axisymmetric FEA model was employed for comparison.

In order to model the viscoelastic pulmonary artery behavior as a function of time, Abaqus 6.10 CAE was used for both creation of the physical model and for the simulation. The

objective of this analysis was to determine the ultimate response of the pulmonary tissue under the prescribed loading conditions. Also, the amount of time necessary to reach this equilibrium will be noted.

The main pulmonary artery was modeled as to retain consistency with the earlier experiments. In this analysis, the tube cross-section was modeled and the problem was defined as axisymmetric. It was assumed that there was no dependence of direction on material behavior in the r, θ, or z directions. This assumption greatly reduced the size of the problem matrix allowing the problem to be run for long periods of time. The artery was modeled using approximate experimental dimensions for the bovine main pulmonary artery. The radial thickness of the artery was assumed to be 5 millimeters while the inner diameter was 14 millimeters. The height of the artery modeled along the axis of symmetry (z axis) was 1 millimeter. Effectively, a small ring of the artery was modeled due to the axisymmetry of the problem. CAX4H elements were used for the problem as they are 4-node bilinear axisymmetric quadrilateral, hybrid, constant pressure. A total of 20 elements were used in the analysis, each with an edge length of 0.5 millimeters.

Most commercially available FEM allow for the use of popular hyperelastic material models [42]. The Ogden formulation postulates that the strain energy is a function of the principle stretches [1] where:

$$W = W(\lambda_1, \lambda_2, \lambda_3) = \sum_{i=1}^{N} \frac{\mu_i}{\alpha_i} (\lambda_1^{\alpha_1}, \lambda_2^{\alpha_2}, \lambda_3^{\alpha_3} - 3) \tag{4.24}$$

Where the condition for consistency of the model is the following

$$\begin{aligned} 2\mu &= \sum_{i=1}^{N} \mu_i \alpha_i \\ \mu_i \alpha_i &> 0 \end{aligned} \tag{4.25}$$

where μ is the shear modulus of the material in the reference configuration.

It has been suggested that using three pairs of constants ($N = 3$) to (4.25) are enough to give excellent correlation to experimental soft tissue data [3]. By applying the Ogden function (4.24) to calculate the stress in the vessel, we have the following:

$$\sigma_1 = \sigma_2 = \frac{\partial W}{\partial \lambda_1} = \frac{\partial W}{\partial \lambda_2} = \sum_{i=1}^{3} \mu_i (\lambda^{\alpha_i} - \lambda^{-2\alpha_i}) \tag{4.26}$$

where a total of six material parameters are used to fit the experimental data. The fitting parameters can be seen in Table 3 below.

Table 3. Fitting parameters for Ogden material model

i	μ_i (N/m^2)	α_i
1	-833,938	-4.256
2	428,656	-2.737
3	415,164	-5.858

The data fit for the Ogden model compared to the experimental data can be seen in Figure 22 below.

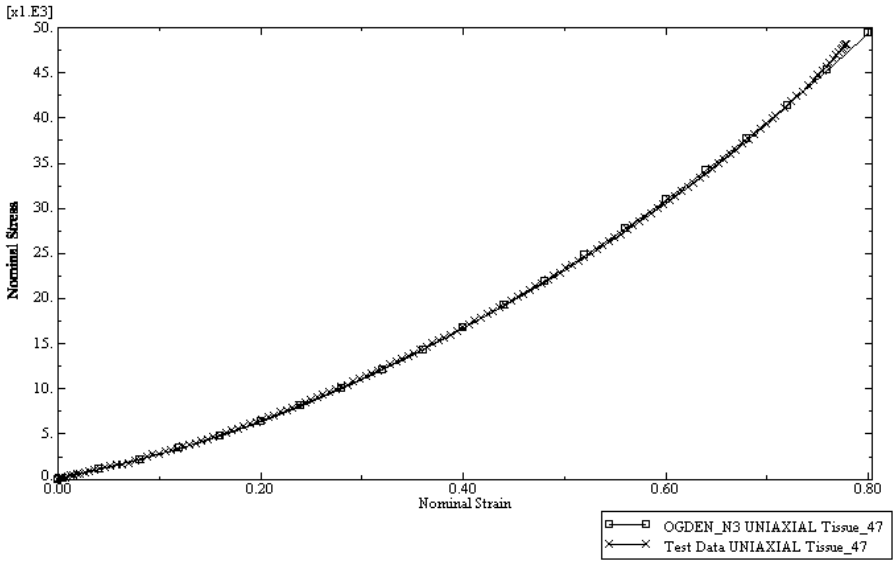

Figure 22. Abaqus model fit for the Ogden material model against experimentally obtained uniaxial stress strain behavior. The Ogden model fits soft tissue very well when using N=3.

In order to incorporate viscoelastic properties into the behavior of the material, the same, five term, Prony series was again used. The fitting parameters from the MPA data were averaged in order to come up with a generalized fit which was used in the Abaqus model. These parameters can be seen in Table 4 below. The moduli for each Prony series (G_i) is normalized by the elastic modulus. The elastic modulus used in this evaluation was E_0 = 66.82 kPa.

Table 4. Experimentally obtained Prony series parameters used for the Abaqus material model

i	***G_i (kPa)***	***τ_i (s)***
1	0.0177	0.39
2	0.0287	2.49
3	0.0320	16.06
4	0.0419	86.11
5	0.1280	803.50

Finally, the density of the vessel wall was assumed to be roughly the density of water, or 1000 kg/m^3.

The loading conditions were now able to be set for the model. The first step of the simulation was a ramp to the average of diastolic and systolic pressure. This resting pressure was set to be 13 kPa, and was applied to only the inner surface of the membrane. Both the upper and lower surfaces of the artery slice were fixed in the y direction, since the artery as a whole is very long when compared to the thickness of 5 mm. In order for the simulation to run for all conditions, this initial loading portion was extended to take 10 seconds. This allows the displacement of the vessel to not be overly large at any particular time step. The boundary conditions for the second step were applied in the same manner. The difference between the two steps was only the profile of the pressure load. During the alternating pressure step of the simulation, the pulsatile nature of blood pressure was simulated. In order to simply capture this phenomenon, a sine wave pressure was applied to the inner surface of the arterial wall. The sine wave amplitude was 3 kPa and oscillated between 10 and 16 kPa. These values correspond to roughly 75 mmHg and 120 mmHg, which are relatively standard diastolic and systolic blood pressure values. The applied pressure profile can be seen in Figure 23.

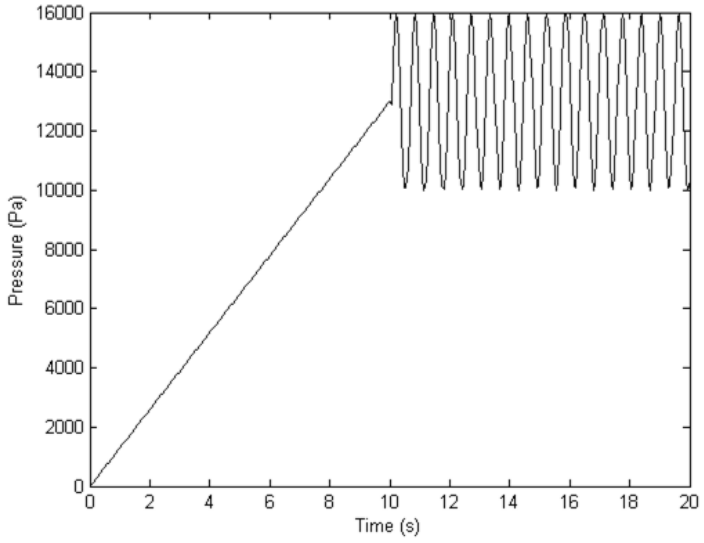

Figure 23. Applied pressure profile used for the finite element simulations. There is an initial loading ramp followed by a sine oscillation at about 95 Hz. The oscillation pressures vary from 10 kPa to 16 kPa or about 80 to 120 mmHg. These parameters are chosen to simulate biological loading conditions.

The Ogden material model simulations were run for 100, 1000, and finally 10,000 seconds within Abaqus standard. The input file for the 10,000 second simulation can be found in the appendix. The analysis produced results which agreed with our hypotheses. The applied pressure produced radial displacements between about 5 and 6 mm. This means that the inner arterial diameter increased from 28 mm to about 40 mm at full systole. This agrees with our previous model, stating that the artery strains grow to around 40% during peak pressure. Also, the strains in both the 2 and 3 directions were confirmed to be approximately zero, which agrees with expected results given the prescribed boundary conditions of the problem. The stress profile contour at peak deformation can be seen below in Figure 24.

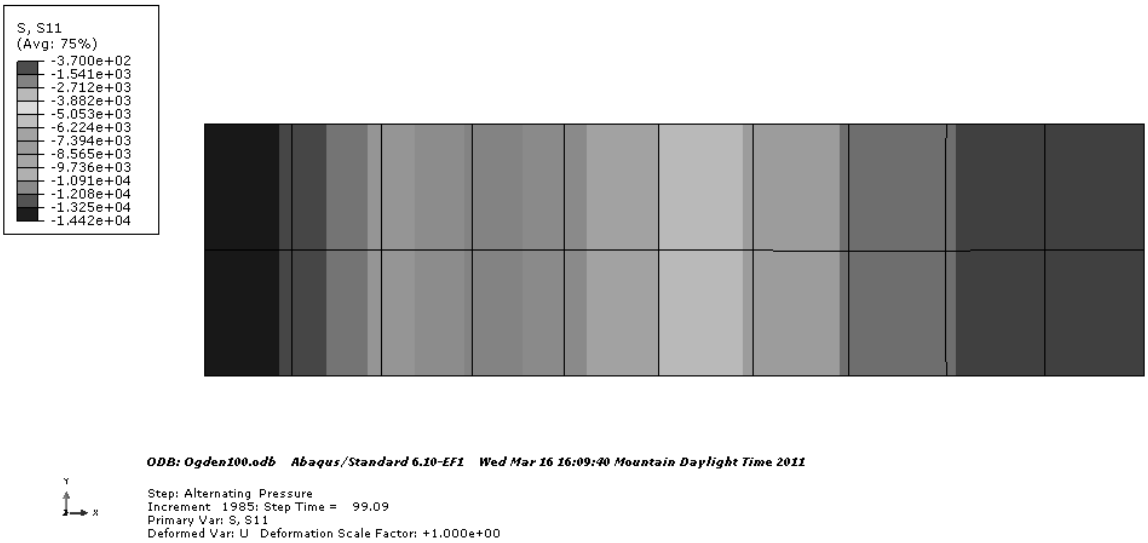

Figure 24. The stress profile contour plot of the arterial section at peak deformation. The stress decreases from about 14.4 kPa on the inner surface of the vessel to 0.37 kPa seen by the outer surface of the wall.

Similarly, the profile of the strain in the 1 direction can be seen below. This direction corresponds to the radial direction, or the direction in which displacement is most greatly affected by the internal pressure. As previously mentioned, the strain in each of the other directions was zero, as prescribed by the initial conditions.

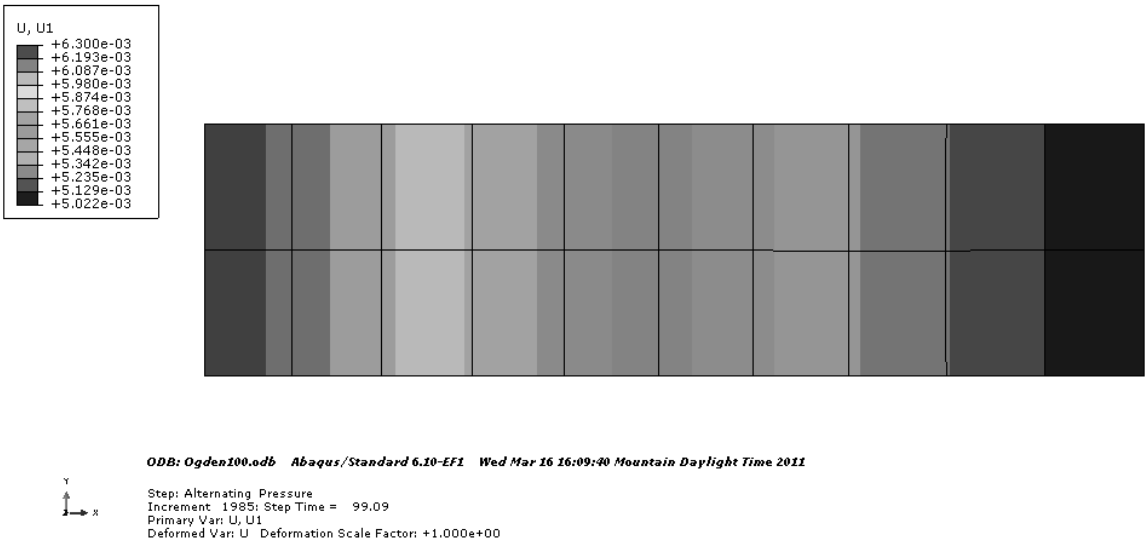

Figure 25. The displacement profile contour plot of the arterial section at peak deformation. The displacement decreases from about 6.3 mm on the inner surface of the vessel to 5.0 mm along the exterior of the wall. These displacements compare favorably with the findings in Chapter III.

The data from the Abaqus simulations with the Ogden material model was then compiled into Matlab in order to observe the pressure-diameter loop and compare it to the P-D loop seen in the results of Chapter III. The diameter was calculated based on the initial internal dimensions of the artery and the radial displacement. A plot of the full pressure-diameter profile can be seen in Figure 26. Also, the loops at 100, 1000, and 10,000 seconds are plotted in order to give some reference as to the time dependence of the tissue. At 10,000 seconds the artery has reached steady state, where the pressure-diameter loop is repeatable.

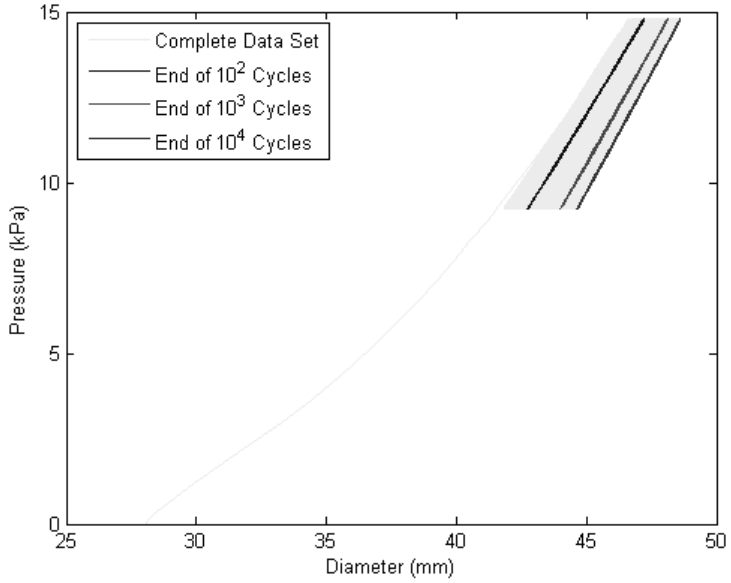

Figure 26. The pressure-diameter response for the Ogden model using the parameters listed in Table 3. The diameter was calculated using the initial radius and the displacement data. It can be seen that the artery does relax from 100 to 1000 seconds and again from 1000 seconds to 10,000 seconds. The artery P-D response is at steady state after 10,000 seconds and reaches a repeatable loop.

In order to compare these results to the Matlab simulations in Chapter III, an additional Prony series term was again added in order to account for the affects of the smooth muscle cells. The same Ogden material model from above was modified as follows. The time constant used was equal to the fastest time constant from Table 2, or $\tau_{smooth} = 0.39$ seconds. From the results seen in Figure 21, it was determined that the modulus corresponding to the smooth muscle cell would be 20 percent of the elastic modulus, E_0. The results of the P-D response, for the FEA simulation incorporating the smooth muscle effects, are shown in Figure 27 below.

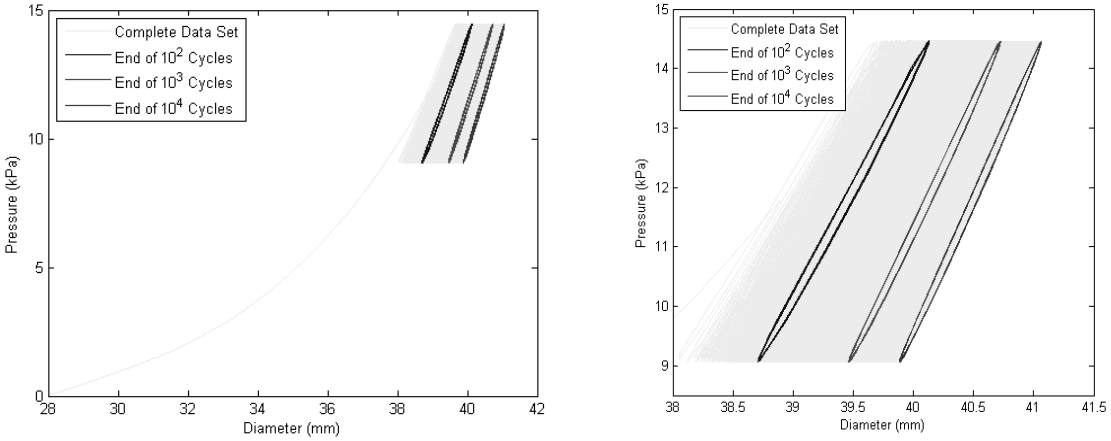

Figure 27. The pressure-diameter response for the modified Ogden model using the parameters listed in Table 3 as well as a smooth muscle term. The smooth term was just an added Maxwell element with a time constant equal to τ_1 (0.39sec) and a modulus value equal to 20% of E_0 (13.36 kPa). The diameter was calculated using the initial radius and the displacement data. It can be seen that the artery does relax from 100 to 1000 seconds and again from 1000 seconds to 10,000 seconds. The artery P-D response is at steady state after 10,000 seconds and reaches a repeatable loop. In the case of the added smooth muscle term it is obvious from the plot on the right that some sort of P-D loop does indeed exist. These results agree favorably with those seen from the Matlab simulations in Chapter III.

The addition of the smooth muscle term did have a slight affect on the pressure-diameter response. When comparing Figure 26 and Figure 27, it is easy to notice that the addition of this term creates a small loop in the response. Although the loop is very small, and not greatly pronounced, it does show the effect of viscoelasticity on the tissue's mechanical response. These FEA simulation results agree well with those previously achieved from the analytical model (shown in Figure 19). The FEA model shows the same overall relaxation effect of the vascular tissue, however again, it seems logical that our above constitutive model could be applied in order to accurately describe the *in vivo* behavior. Even with the addition of the smooth muscle effect, the hysteresis loop seen in the P-D curve is minimal, and thus could in most cases probably be ignored.

CHAPTER V

V. Conclusion

Cardiovascular modeling continues to be a very active field of research as both mechanical and computational models advance [1]. The motivation of these models is generally that of cardiac disease, as it is hopeful that further understanding of arterial behavior and mechanics could help with the design of treatment techniques. Namely, arterial modeling takes into account the flexibility of the vessel wall which could help in the design and application of stents and bypasses.

The behavior of bovine pulmonary arteries including preconditioning behavior and viscoelastic response were observed and quantified. It has been well established that soft tissues do indeed exhibit some degree of viscoelastic nature, however the importance or physiologic role of this viscoelasticity has only been speculated [7, 10, 11, 20, 24-38]. It is also widely accepted that in order to create a more accurate model describing the behavior of soft tissues, viscoelasticity must be considered. This work delves into the effect of viscoelasticity and the importance of considering viscoelasticity of pulmonary arteries subjected to *in vivo* loading conditions.

The viscoelastic behavior of bovine pulmonary arteries was observed and a simple model describing this behavior was presented and verified through both an analytical model and finite element simulation. The stress relaxation curves of the artery were fit with a 5 term Prony series in order to determine the individual relaxation times of the material. The characterization of the viscoelastic response was then simplified through the use of the Boltzmann integral. Given the *in vivo* boundary conditions, this integral then simplified to a cosine term, which is independent

of the relaxation time. This simplified model was dependent only on the Prony series modulus and matched the ultimate stress response of the arteries very well.

The results from this simplified model and the analytical Matlab model were then verified through finite element simulation. By comparing the pressure-diameter curves of the FEA simulation to the predicted stress-strain response of the analytical model, it was observed that the ultimate response was nearly identical in each case. In both cases, the addition of a smooth muscle term did in fact increase the amount of hysteresis seen at ultimate response; however the loop was still small enough that under most loading cases it could be assumed negligible.

BIBLIOGRAPHY

1. Kalita, P. and R. Schaefer, *Mechanical Models of Artery Walls.* Archives of Computational Methods in Engineering, 2008. **15**(1): p. 1-36.

2. Hokanson, J. and S. Yazdani, *A constitutive model of the artery with damage.* Mechanics Research Communications, 1996. **24**(2): p. 151-159.

3. Holzapfel, G., T. Gasser, and R. Ogden, *A New Constitutive Framework for Arterial Wall Mechanics and a Comparative Study of Material Models.* Journal of Elasticity, 2000. **61**(1): p. 1-48.

4. Tzikang, C., *Determining a Prony Series for a Viscoelastic Material From Time Varying Strain Data*. 2000, NASA Langley Technical Report Server.

5. Qi, H.J. and P.H. Kao, *A Microstructually-Driven Model for Pulmonary Artery Tissue.* Journal of Biomechanical Engineering, Accepted Manuscript October 4, 2010.

6. Carew, E.O., et al., *Stress Relaxation Preconditioning of Porcine Aortic Valves.* Annals of Biomedical Engineering, 2004. **32**(4): p. 563-572.

7. Grashow, J., et al., *Planar Biaxial Creep and Stress Relaxation of the Mitral Valve Anterior Leaflet.* Annals of Biomedical Engineering, 2006. **34**(10): p. 1509-1518.

8. Liu, Z. and K. Yeung, *The Preconditioning and Stress Relaxation of Skin Tissue.* Biomedical & Pharmaceutical Engineering, 2006. **2**(1): p. 22-28.

9. Sverdlik, A. and Y. Lanir, *Time-Dependent Mechanical Behavior of Sheep Digital Tendons, Including the Effects of Preconditioning.* Journal of Biomechanical Engineering, 2002. **124**(1): p. 78-84.

10. Hingorani, R.V., et al., *Nonlinear Viscoelasticity in Rabbit Medial Collateral Ligament.* Annals of Biomedical Engineering, 2004. **32**(2): p. 306-312.

11. Provenzano, P.P., et al., *Application of nonlinear viscoelastic models to describe ligament behavior.* Biomechanics and Modeling in Mechanobiology, 2002. **1**(1): p. 45-57.

12. Einat, R. and L. Yoram, *Recruitment Viscoelasticity of the Tendon.* Journal of Biomechanical Engineering, 2009. **131**(11): p. 111008-8.

13. Cox, R.H., *Viscoelastic properties of canine pulmonary arteries.* The American Journal of Physiology, 1984. **15**(1): p. 7.

14. Humphrey, J.D., *Cardiovascular Solid Mechanics*. 1 ed. 2002: Springer. 776.

15. Holzapfel, G.A., *Structural and numerical models for the (visco)elastic response of arterial walls with residual stresses.*, in *Biomechanics of soft tissue in cardiovascular system*, G.A. Holzapfel and R.W. Ogden, Editors. 2003, Springer: New York. p. 109-184.

16. Hayashi, K., *Mechanical properties of soft tissues and arterial walls.*, in *Biomechanics of soft tissue in cardiovascular system*, G.A. Holzapfel and R.W. Ogden, Editors. 2003, Springer: New York. p. 15-64.

17. Fung, Y.C., *Biomechanics: Mechanical Properties of Living Tissues*. 2 ed. 1993, New York: Springer.

18. Giles, J.M., A.E. Black, and J.E. Bischoff, *Anomalous rate dependence of the preconditioned response of soft tissue during load controlled deformation.* Journal of Biomechanics, 2007. **40**(4): p. 777-785.

19. Cheng, S., E.C. Clarke, and L.E. Bilston, *The effects of preconditioning strain on measured tissue properties.* Journal of Biomechanics, 2009. **42**(9): p. 1360-1362.

20. Holzapfel, G.A., T.C. Gasser, and M. Stadler, *A structural model for the viscoelastic behavior of arterial walls: Continuum formulation and finite element analysis.* European Journal of Mechanics - A/Solids, 2002. **21**(3): p. 441-463.

21. Fiford, R.J. and L.E. Bilston, *The mechanical properties of rat spinal cord in vitro.* Journal of Biomechanics, 2005. **38**(7): p. 1509-1515.

22. Carew, E.O., J.E. Barber, and I. Vesely, *Role of Preconditioning and Recovery Time in Repeated Testing of Aortic Valve Tissues: Validation Through Quasilinear Viscoelastic Theory.* Annals of Biomedical Engineering, 2000. **28**(9): p. 1093-1100.

23. Gefen, A., et al., *Age-Dependent Changes in Material Properties of the Brain and Braincase of the Rat.* Journal of Neurotrauma, 2003. **20**(11): p. 1163-1177.

24. Armentano, R., et al., *Effects of Hypertension on Viscoelasticity of Carotid and Femoral Arteries in Humans.* Hypertension, 1995. **26**(1): p. 48-54.

25. Armentano, R.L., et al., *Arterial Wall Mechanics in Conscious Dogs : Assessment of Viscous, Inertial, and Elastic Moduli to Characterize Aortic Wall Behavior.* Circ Res, 1995. **76**(3): p. 468-478.

26. Bagley, R.L. and P.J. Torvik, *A Theoretical Basis for the Application of Fractional Calculus to Viscoelasticity.* Journal of Rheology, 1983. **27**(3): p. 201-210.

27. Čanić, S., et al., *Modeling Viscoelastic Behavior of Arterial Walls and Their Interaction with Pulsatile Blood Flow.* SIAM Journal on Applied Mathematics, 2006. **67**(1): p. 164-193.

28. Craiem, D., et al., *Fractional-order viscoelasticity applied to describe uniaxial stress relaxation of human arteries.* Physics in Medicine and Biology, 2008. **53**: p. 4543-4554.

29. Doehring, T.C., E.O. Carew, and I. Vesely, *The Effect of Strain Rate on the Viscoelastic Response of Aortic Valve Tissue: A Direct-Fit Approach.* Annals of Biomedical Engineering, 2004. **32**(2): p. 223-232.

30. Ingomar, L.J.g., *Viscoelastic behavior of organic materials: consequences of a logarithmic dependence of force on strain rate.* Journal of Biomechanics, 2005. **38**(7): p. 1451-1458.

31. Kang, T., *Mechanical behavior of arteries under inflation and extension.* Journal of Mechanical Science and Technology, 2008. **22**(4): p. 621-627.

32. Rousseau, E.P.M., et al., *Elastic and viscoelastic material behaviour of fresh and glutaraldehyde-treated porcine aortic valve tissue.* Journal of Biomechanics, 1983. **16**(5): p. 339-341, 343-348.

33. Sasaki, N., et al., *Stress relaxation function of bone and bone collagen.* Journal of Biomechanics, 1993. **26**(12): p. 1369-76.

34. Shau, Y.-W., et al., *Noninvasive assessment of the viscoelasticity of peripheral arteries.* Ultrasound in Medicine & Biology, 1999. **25**(9): p. 1377-1388.

35. Taha, M.M.R., S. Neidigk, and A. Noureldin, *Variable stiffness rheological model for interrelating creep and stress relaxation in ligaments.* International Journal of Experimental and Computational Biomechanics, 2009. **1**: p. 96-113.

36. Toms, S.R., et al., *Quasi-linear viscoelastic behavior of the human periodontal ligament.* Journal of Biomechanics, 2002. **35**(10): p. 1411-1415.

37. Zatzman, M., et al., *Time Course of Stress Relaxation in Isolated Arterial Segments.* Am J Physiol, 1954. **177**(2): p. 299-302.

38. Zhang, W., Y. Liu, and G.S. Kassab, *Viscoelasticity reduces the dynamic stresses and strains in the vessel wall: implications for vessel fatigue.* Am J Physiol Heart Circ Physiol, 2007. **293**(4): p. H2355-2360.

39. Craiem, D. and R. Armentano, *A fractional derivative model to describe arterial viscoelasticity.* Biorheology, 2007. **44**(4).

40. Cowin, S.C., *How Is a Tissue Built?* Journal of Biomechanical Engineering, 2000. **122**(6): p. 553-569.

41. Kanner, L.M. and C.O. Horgan, *Elastic instabilities for strain-stiffening rubber-like spherical and cylindrical thin shells under inflation.* International Journal of Non-Linear Mechanics, 2007. **42**(2): p. 204-215.

42. Sponagel, S., et al., *Experiment and material model for soft tissue materials*, in *Constitutive Models for Rubber VI*. 2009, CRC Press. p. 465-470.

APPENDIX

Analytical Matlab Model

```
%function name: viscoAnalytical
%Analytical model of viscoelastsic behavior
 clear all
 close all
 clc

%Model Input Parameters
 E1 = 1.18;
 E2 = 1.92;
 E3 = 2.14;
 E4 = 2.80;
 E5 = 8.55;
 E0 = 66.82;
 tao1 = 0.39;
 tao2 = 2.49;
 tao3 = 16.06;
 tao4 = 86.11;
 tao5 = 803.50;

%loading parameters
 time1 = (0:0.01:100);
 time2 = (100.1:.1:1e5);
 time = [time1,time2];
 t1 = time(1:300);
 t2 = time(301:end);

 e1 = (4/30).*time;    %define intitial loading ramp
 e1 = e1(1:300);
 e2 = 0.3 + 0.1*cos(10.*(t2-3));   %define cyclic loading

 strain = [e1,e2];   %define total strain input

 syms s t

%solving the linear portion for t<3
 stress001 = E1*(int(exp(-(t-s)/tao1)*(4/30),s,0,t));
 s001 = subs(stress001,t1);

 stress002 = E2*(int(exp(-(t-s)/tao2)*(4/30),s,0,t));
 s002 = subs(stress002,t1);

 stress003 = E3*(int(exp(-(t-s)/tao3)*(4/30),s,0,t));
 s003 = subs(stress003,t1);

 stress004 = E4*(int(exp(-(t-s)/tao4)*(4/30),s,0,t));
 s004 = subs(stress004,t1);

 stress005 = E5*(int(exp(-(t-s)/tao5)*(4/30),s,0,t));
 s005 = subs(stress005,t1);

%solving the linear portion for t>=3
```

```
 stress01 = E1*(int(exp(-(t-s)/tao1)*(4/30),s,0,3));
 s01 = subs(stress01,t2);

 stress02 = E2*(int(exp(-(t-s)/tao2)*(4/30),s,0,3));
 s02 = subs(stress02,t2);

 stress03 = E3*(int(exp(-(t-s)/tao3)*(4/30),s,0,3));
 s03 = subs(stress03,t2);

 stress04 = E4*(int(exp(-(t-s)/tao4)*(4/30),s,0,3));
 s04 = subs(stress04,t2);

 stress05 = E5*(int(exp(-(t-s)/tao5)*(4/30),s,0,3));
 s05 = subs(stress05,t2);

%solving the cyclic portion for t>=3
 stress11 = E1*(int(exp(-(t-s)/tao1)*(-sin(10*s-30)),s,3,t));
 s11 = subs(stress11,t2);

 stress12 = E2*(int(exp(-(t-s)/tao2)*(-sin(10*s-30)),s,3,t));
 s12 = subs(stress12,t2);

 stress13 = E3*(int(exp(-(t-s)/tao3)*(-sin(10*s-30)),s,3,t));
 s13 = subs(stress13,t2);

 stress14 = E4*(int(exp(-(t-s)/tao4)*(-sin(10*s-30)),s,3,t));
 s14 = subs(stress14,t2);

 stress15 = E5*(int(exp(-(t-s)/tao5)*(-sin(10*s-30)),s,3,t));
 s15 = subs(stress15,t2);

%combine stress values to get total stress for all times
 s1 = [s001, s01+s11];
 s2 = [s002, s02+s12];
 s3 = [s003, s03+s13];
 s4 = [s004, s04+s14];
 s5 = [s005, s05+s15];

 s0 = E0*strain;   %define stress due to linear element

 sT = s0 + s1 + s2 + s3 + s4 + s5;   %define total stress

%simplified stresses as t approaches infinity
 simp1 = 0.1*E1*cos(10*t2-30);
 simp2 = 0.1*E2*cos(10*t2-30);
 simp3 = 0.1*E3*cos(10*t2-30);
 simp4 = 0.1*E4*cos(10*t2-30);
 simp5 = 0.1*E5*cos(10*t2-30);

%total simplified stress
 simpT = s0(301:end) + simp1 + simp2 + simp3 + simp4 + simp5;
 y = [0,  max(s0)];
 x = [0, 0.4];

%plot of first element branch with simplified response
 subplot(3,2,1);
 plot(strain,s1,'b');
```

```
 hold on
 plot(strain(301:end),simp1,'k');
 title('Branch 1');
 xlabel('Strain');
 ylabel('Stress (kPa)');

%plot of second element branch with simplified response
 subplot(3,2,2);
 plot(strain,s2,'b');
 hold on
 plot(strain(301:end),simp2,'k');
 title('Branch 2');
 xlabel('Strain');
 ylabel('Stress (kPa)');

%plot of third element branch with simplified response
 subplot(3,2,3);
 plot(strain,s3,'b');
 hold on
 plot(strain(301:end),simp3,'k');
 title('Branch 3');
 xlabel('Strain');
 ylabel('Stress (kPa)');

%plot of forth element branch with simplified response
 subplot(3,2,4);
 plot(strain,s4,'b');
 hold on
 plot(strain(301:end),simp4,'k');
 title('Branch 4');
 xlabel('Strain');
 ylabel('Stress (kPa)');

%plot of fifth element branch with simplified response
 subplot(3,2,5.5);
 plot(strain,s5,'b');
 hold on
 plot(strain(301:end),simp5,'k');
 title('Branch 5');
 xlabel('Strain');
 ylabel('Stress (kPa)');

%plot total response with simplified response
 figure (2)
 plot(strain,sT,'b');
 hold on
 plot(strain(301:end),simpT,'k');
 plot(x,y,'c');
 title('Total Stress');
 xlabel('Strain');
 ylabel('Stress (kPa)');
```

Abaqus Input File

```
*Heading
** Job name: Ogden Model name: BovinePulmonary
** Generated by: Abaqus/CAE 6.10-EF1
*Preprint, echo=NO, model=NO, history=NO, contact=NO
**
** PARTS
**
*Part, name=Vessel
*Node
      1, 0.0189999994, 0.00400000019
      2, 0.0140000004, 0.00400000019
      3, 0.0140000004, 0.00300000003
      4, 0.0189999994, 0.00300000003
      5, 0.0185000002, 0.00400000019
      6, 0.0179999992, 0.00400000019
      7, 0.0175000001, 0.00400000019
      8, 0.0170000009, 0.00400000019
      9, 0.0164999999, 0.00400000019
     10, 0.0160000008, 0.00400000019
     11, 0.0154999997, 0.00400000019
     12, 0.0149999997, 0.00400000019
     13, 0.0144999996, 0.00400000019
     14, 0.0140000004, 0.00350000011
     15, 0.0144999996, 0.00300000003
     16, 0.0149999997, 0.00300000003
     17, 0.0154999997, 0.00300000003
     18, 0.0160000008, 0.00300000003
     19, 0.0164999999, 0.00300000003
     20, 0.0170000009, 0.00300000003
     21, 0.0175000001, 0.00300000003
     22, 0.0179999992, 0.00300000003
     23, 0.0185000002, 0.00300000003
     24, 0.0189999994, 0.00350000011
     25, 0.0179997738, 0.00349709298
     26, 0.0159999002, 0.00349781476
     27, 0.0149999503,  0.003498815
     28, 0.0184999574, 0.0034990923
     29,  0.017499797, 0.00349698099
     30, 0.0169999022, 0.00349777634
     31, 0.0154999718, 0.00349894725
     32, 0.0164999627, 0.00349862291
     33, 0.0144999903, 0.00349962991
*Element, type=CAX4H
 1,  5, 28, 24,  1
 2,  6, 25, 28,  5
 3, 25, 29, 21, 22
 4,  8, 30, 29,  7
 5, 18, 19, 32, 26
 6, 26, 31, 17, 18
 7, 12, 27, 31, 11
 8, 31, 27, 16, 17
 9, 13, 33, 27, 12
10, 27, 33, 15, 16
11,  2, 14, 33, 13
12,  3, 15, 33, 14
```

```
13,  9, 32, 30,  8
14, 30, 32, 19, 20
15, 29, 30, 20, 21
16,  7, 29, 25,  6
17, 22, 23, 28, 25
18, 23,  4, 24, 28
19, 26, 10, 11, 31
20, 32,  9, 10, 26
*Nset, nset=_PickedSet2, internal, generate
  1,  33,   1
*Elset, elset=_PickedSet2, internal, generate
  1,  20,   1
** Section: TissueSection
*Solid Section, elset=_PickedSet2, material=Tissue
,
*End Part
**
**
** ASSEMBLY
**
*Assembly, name=Assembly
**
*Instance, name=Vessel-1, part=Vessel
*End Instance
**
*Nset, nset=_PickedSet11, internal, instance=Vessel-1
  1,  2,  3,  4,  5,  6,  7,  8,  9, 10, 11, 12, 13, 15, 16, 17
 18, 19, 20, 21, 22, 23
*Elset, elset=_PickedSet11, internal, instance=Vessel-1, generate
  1,  20,   1
*Nset, nset=Set-1, instance=Vessel-1
  2,  3, 14
*Elset, elset=Set-1, instance=Vessel-1
 11, 12
*Elset, elset=__PickedSurf10_S1, internal, instance=Vessel-1
 11,
*Elset, elset=__PickedSurf10_S4, internal, instance=Vessel-1
 12,
*Surface, type=ELEMENT, name=_PickedSurf10, internal
__PickedSurf10_S1, S1
__PickedSurf10_S4, S4
*Elset, elset=__PickedSurf13_S1, internal, instance=Vessel-1
 11,
*Elset, elset=__PickedSurf13_S4, internal, instance=Vessel-1
 12,
*Surface, type=ELEMENT, name=_PickedSurf13, internal
__PickedSurf13_S1, S1
__PickedSurf13_S4, S4
*End Assembly
*Amplitude, name=Amp-1, time=TOTAL TIME, definition=PERIODIC
1,          10.,           1.,         4.33
          1.,           0.
*Amplitude, name=Ramp
          0.,           0.,          10.,           1.
**
** MATERIALS
**
```

```
** Bovine Pulmonary Tissue
*Material, name=Tissue
*Density
1000.,
*Hyperelastic, n=3, ogden, moduli=LONG TERM
-833938., -4.256,428656., -2.737,415164., -5.858,     0.,     0.
     0.,
*Viscoelastic, time=PRONY
 0.0176594,    0.,  0.39
 0.0287339,    0.,  2.49
 0.0320263,    0., 16.06
 0.0419036,    0., 86.11
  0.127956,    0., 803.5
** ----------------------------------------------------------------
**
** STEP: Pressure Ramp
**
*Step, name="Pressure Ramp", nlgeom=YES
*Visco, cetol=0.05
0.5, 10., 0.001, 0.5
**
** BOUNDARY CONDITIONS
**
** Name: BC-2 Type: Displacement/Rotation
*Boundary
_PickedSet11, 2, 2
**
** LOADS
**
** Name: Ramp Pressure   Type: Pressure
*Dsload, amplitude=Ramp
_PickedSurf10, P, 13000.
**
** OUTPUT REQUESTS
**
*Restart, write, frequency=0
*Print, solve=NO
**
** FIELD OUTPUT: F-Output-2
**
*Output, field
*Node Output
U,
*Element Output, directions=YES
S,
**
** HISTORY OUTPUT: H-Output-2
**
*Output, history
*Energy Output
ETOTAL,
*End Step
** ----------------------------------------------------------------
**
** STEP: Alternating  Pressure
**
*Step, name="Alternating  Pressure", nlgeom=YES, inc=1000000
```

```
*Visco, cetol=0.05
0.01, 10000., 0.0001, 0.05
**
** LOADS
**
** Name: Ramp Pressure   Type: Pressure
*Dsload, op=NEW
** Name: alternating pressure   Type: Pressure
*Dsload, op=NEW, amplitude=Amp-1
_PickedSurf13, P, 3000.
**
** OUTPUT REQUESTS
**
*Restart, write, frequency=0
**
** FIELD OUTPUT: F-Output-2
**
*Output, field
*Node Output
U,
*Element Output, directions=YES
E, S
**
** HISTORY OUTPUT: H-Output-2
**
*Output, history
*Energy Output
ETOTAL,
*End Step
```